6-1-1992

FAGE Measurements of Tropospheric HO with Measurements and Model of Interferences

Thomas M. Hard
Portland State University

A. A. Mehrabzadeh
Portland State University

C. Y. Chan
Portland State University

Robert J. O'Brien
Portland State University

Citation Details

Hard, T. M., Mehrabzadeh, A. A., Chan, C. Y., and O'Brien, R. J. (1992). FAGE measurements of tropospheric HO with measurements and model of interferences. Journal Of Geophysical Research, 97(D9), 9795-9817.

JOURNAL OF GEOPHYSICAL RESEARCH, VOL. 97, NO. D9, PAGES 9795–9817, JUNE 20, 1992

FAGE Measurements of Tropospheric HO With Measurements and Model of Interferences

T. M. HARD, A. A. MEHRABZADEH, C. Y. CHAN, AND R. J. O'BRIEN

Chemistry Department and Environmental Sciences and Resources Program, Portland State University, Portland, Oregon

Ambient HO measurements by low-pressure laser-excited fluorescence with chemical modulation, and supporting ozone and water-vapor data, are presented for periods in May and August 1987. The observed peak daytime ambient HO concentrations are in the range (2.5 to 8)$\times 10^6$ molecules cm^{-3} and show small negative offsets due to photochemical interference. Direct measurements of the interference at fixed [O_3] give the dependence on ambient [H_2O] and on the modulating reagent [isobutane]. At ambient [O_3]=30 ppb and 10 torr H_2O, with excitation and detection at a total pressure of 4 torr, the net interference is equal to [HO]$=-1.3\times 10^6$ molecule cm^{-3}. Production of HO by the reaction of isobutane with O(^1D) accounts for the negative interference. Quenching of HO fluorescence by the modulating reagent contributes a smaller positive term to the interference; kinetic measurements of the quenching rate coefficient yield $k_{Q\Phi}$(HO A ($v'=0$) + isobutane) = (1.0±0.15) $\times 10^{-9}$ cm^3 molecule^{-1} s^{-1}. The experimental interference results are compared with a detailed kinetic model of HO production, excitation, relaxation, and detection; reasonable agreement is found despite uncertainties in beam spatial and temporal profiles and in the rate coefficients necessary to the model. The model also computes the interference due to H_2O_2 photolysis. Net interference and signal-to-noise ratio are computed as functions of photon flux for 1,0 (YAG/dye 282 nm) and 0,0 (Cu/dye 308 nm) excitation.

INTRODUCTION

The hydroxyl radical HO controls the atmospheric fates of most trace gases emitted into the Earth's atmosphere by nature and by human technology. These trace gases in turn influence the environment at the Earth's surface via their effects on its temperature and on photochemically and biologically active radiation. Measurements of atmospheric HO concentrations thus can assist in the evaluation of the resilience of the atmosphere to human-induced chemical changes.

In the past we have reported diurnal HO measurements [*Hard et al.*, 1986] in relatively unpolluted urban air. Following those experiments we have moved the instrument to a mobile laboratory located at a clean-air site on the Oregon coast. Ambient HO data from that site are presented here for two continuous periods of more than 48 hours. The observed HO concentrations are comparable with those reported in 1986.

Some of the earlier data showed a negative offset at night. The present data show negative nighttime offsets which roughly correlate with ozone concentrations. With laboratory measurements and with a photochemical model we elucidate the sources of these offsets and determine instrumental modifications that can reduce them to negligible levels.

In the determination of ambient hydroxyl radical by laser-excited fluorescence (LEF), production of spurious HO by the laser has been a matter of continuing concern [*Hanabusa et al.*, 1977; *Hard et al.*, 1980; *Ortgies et al.*, 1981; *Davis et al.*, 1981*a*, *b*; *Wang et al.*, 1981; *Wang and Davis*, 1982; *Shirinzadeh et al.*, 1987*a*; *Smith and Crosley*, 1990].

Paper number 91JD01664.
0148-0227/92/91JD-01664$05.00

To combat this spurious signal, we have developed a low-pressure measurement technique termed FAGE [*Hard et al.*, 1980, FAGE1 [*Hard et al.*, 1984], and FAGE2 [*Hard et al.*, 1986], which greatly reduces this interference, relative to excitation at atmospheric pressure. In a previous measurement of ambient HO in urban air using FAGE2 [*Hard et al.*, 1986] we subtracted the negative offset of -2×10^5 cm^{-3} from our November 1985 data. Such an offset was not apparent in that paper's summer data, where HO concentrations were much higher. Unfortunately, ozone measurements were not available to complement those data, due to instrument malfunction, and thus the offsets could not be correlated with possible photochemical interferences.

However, in our experiments at the coastal site, ambient ozone, water vapor, and other variables have been measured along with HO, as shown in Figure 1. These data, as well as other ambient data not included here, show the presence of small negative signals during the night, when HO is expected to be quite low in concentration. Experiments reported here indicate that these negative signals are largely due to the reaction of O(^1D), produced in laser photolysis of ozone, with the isobutane reagent to produce spurious HO in the background channel. Since the two-channel FAGE2 instrument provides continuous signal and background measurements, with alternating roles of each channel, any offset, positive or negative, must be associated with the isobutane used to remove HO from the background channel. Although smaller than the measured daily maximum HO concentrations, these signals are troublesome. In this paper we investigate the detailed nature of these negative signals experimentally and theoretically and indicate that modifications of the modulation or excitation method can reduce their magnitude to negligible levels.

The goals of this work have been to (1) measure atmospheric HO concentrations, (2) perform a systematic experimental investigation of photochemical interferences,

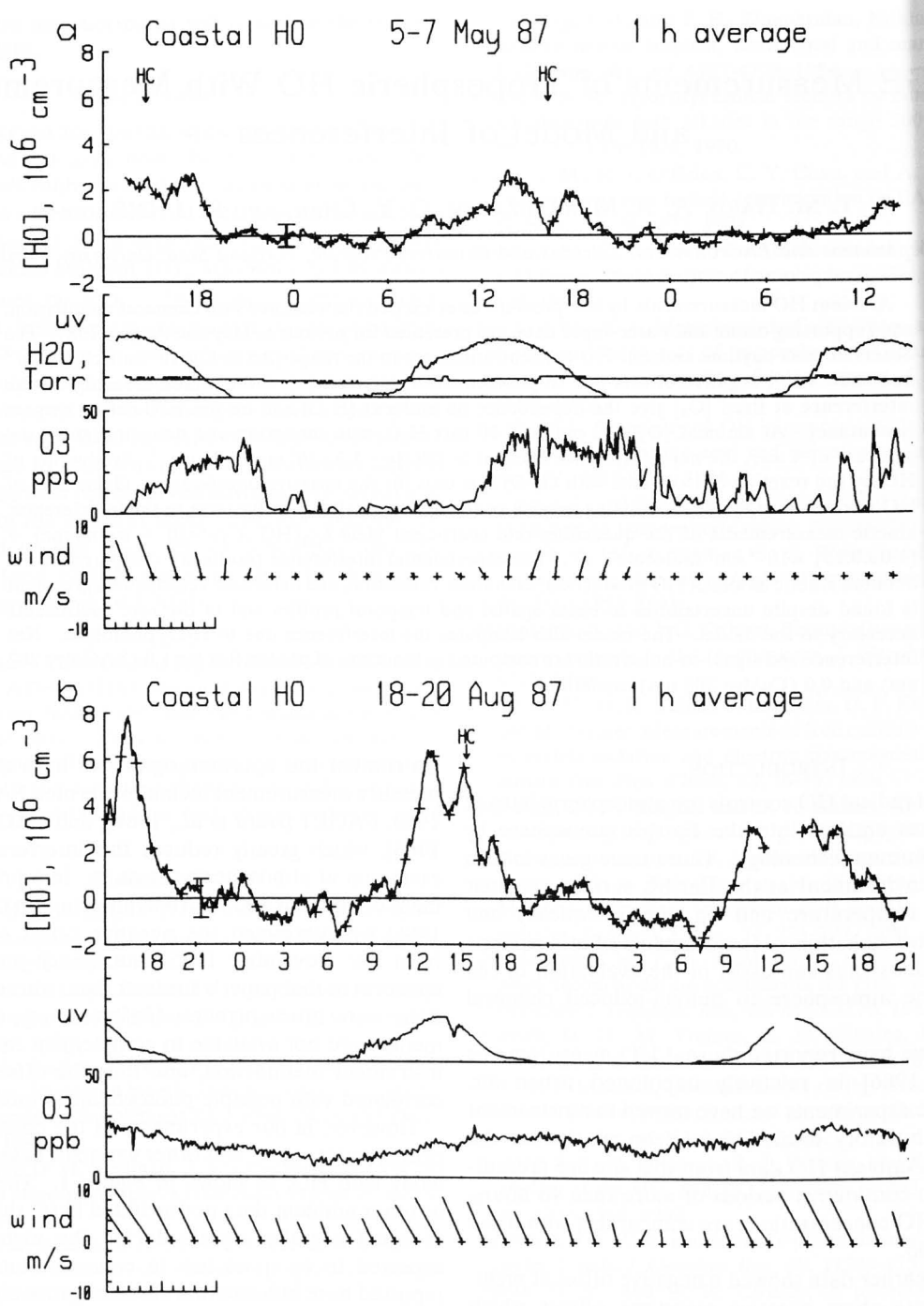

Fig. 1. Ambient HO data measured at coastal site, Lincoln City, Oregon, 45°N 124°W, using FAGE2 instrument with 1-hour averaging time. Vertical error bars represent the value of $\pm 2\epsilon_M$ (equation 3*b*) averaged over each entire HO data set. Arrows indicate times when hydrocarbon grab samples were taken. Supporting UV, H_2O, and O_3 data are not averaged: (*a*) May 5-7, 1987; (*b*) August 18-20, 1987.

(3) develop a qualitative understanding of the relative magnitudes of the several interference processes occurring in these experiments, (4) develop a rigorous model of production, excitation, and fluorescence processes, and (5) utilize the model to determine whether the observed ambient HO signals and experimentally determined negative offsets are consistent with the chemical physical processes governing our measurement technique.

Our earlier work in the detection of atmospheric HO [*Hard et al.*, 1984, 1986] has been criticized by others [*Shirinzadeh et al.*, 1987*a*; *Smith and Crosley*, 1990] for insufficient attention to interferences. We address these criticisms below in the sections entitled "comparison with other models" and "interferences in previous work."

In HO determination by LEF the desired signal is generally smaller than other detected photon signals. The unwanted signals, or backgrounds, can arise from scattering and fluorescence by the instrument walls or by components

of the air sample, from photomultiplier dark current, from chemiluminescence or ambient light, or from HO generated by the action of the UV laser on the air sample. As in all fluorescence measurements, it is necessary to measure the total background in order to obtain the net signal from ambient HO. The background is measured by removing the desired signal, either by tuning the laser away from the chosen absorption line (spectral modulation) or by removal of the ambient HO (chemical modulation). Interferences arise when either modulation method increases or decreases any of the background sources during the attempted measurement. If S is the ambient HO signal, B_1 the total background during signal measurement, B_2 the total background during background measurement, and n the number of equal time intervals of length t over which the signal is averaged, then the experimental measurement of the mean net signal rate M ($\equiv S/nt$) is represented by

$$M = (S + B_1)/nt - B_2/nt \quad (1)$$

and the net interference rate is

$$I/nt = B_1/nt - B_2/nt \quad (2)$$

whose sign is determined by the relative sizes of B_1 and B_2.

Most of this paper addresses the systematic errors collectively represented by I, whose presence can compromise the specificity of an instrument designed to determine a trace species such as HO. However, changes in instrument design to avoid such errors should not be allowed to degrade the instrument's sensitivity, which is a function of the random uncertainties in the measurement process described by equation (1). The random uncertainty in a measurement of the mean net HO signal rate M must be obtained from appropriate statistical treatment of the data. Here we use e_M to represent the standard error of the mean:

$$e_M = (e^2_{(S+B1)/nt} + e^2_{B2/nt} - 2e_{S+B1,\,B2}/nt)^{1/2} \quad (3a)$$

in which the first and second terms on the right are the variances of $(S+B_1)/nt$ and B_2/nt, respectively, and the third term is their covariance. Each of the latter terms can be computed from the data using standard formulas [*Bevington*, 1969]; however, an identical result for e_M is obtained by directly evaluating the uncertainty in the net mean signal rate data, using the usual formula for the standard deviation of the mean:

$$e_M = \{[\Sigma M_i^2 - (\Sigma M_i)^2/n]/(n-1)\}^{1/2} \quad (3b)$$

Various contributions to the uncertainty e_M arise from physical sources of fluctuations in $(S+B_1)$ and B_2. One of these sources is unavoidable when $(S+B_1)$ and B_2 consist of photon counts, whose minimum variance (the Poisson variance) is equal to the number of photons counted. Thus, if we replace the first two terms on the right in equation (3a) with the corresponding Poisson variances, we obtain a lower bound to the value of e_M:

$$(e_M)_{est.1} = ((S+B_1)/(nt)^2 + B_2/(nt)^2 - 2e_{S+B1,\,B2}/(nt))^{1/2} \quad (4a)$$

In analyzing ambient HO signals in our earlier work [*Hard et al.*, 1984, 1986] we omitted the covariance term in equation (4a). Such omission is too conservative, since $(S+B_1)$ and B_2 are strongly correlated. In practice, we have found that the omission of the covariance in equation (4a) gives a value of e_M somewhat larger than we obtain with equation (3a) or equation (3b). In general, if the ambient HO signals have been obtained by subtraction of raw signals consisting of sufficient numbers of photons, and if the net data belong to a Gaussian distribution around the local means, then e_M as given by equation (3b) is the appropriate measure of the uncertainty in the net signal. If, on the other hand, the signals arise not from a real measurement process but from a model, then

$$(e_M)_{est.2} = ((S+B_1) + B_2)^{1/2}/(nt) \quad (4b)$$

is a useful estimate of the uncertainty which appears to be conservative for this instrument. Therefore we now use equation (3b) in the analysis of ambient HO data and equation (4b) in estimating the consequences of possible modifications to the instrument. One measure of such consequences is the signal-to-noise ratio (snr) at a given HO concentration and averaging time. The snr is the ratio of the mean net signal rate M to its uncertainty e_M.

The photochemical reactions leading to ozone interference are

(R1) $O_3 + h\nu$ ($\lambda < 320$ nm) $\rightarrow O_2(^1\Delta_g) + O(^1D_2)$

(R2) $O(^1D) + M\ (N_2, O_2) \rightarrow O(^3P) + M$

(R3) $O(^1D) + H_2O \rightarrow 2\ HO$

When a hydrogen-containing reagent, such as isobutane, is used to modulate ambient HO in a low-pressure flow, the following reaction produces additional HO:

(R4a) $O(^1D)$ + isobutane $\rightarrow$ HO + {i-butyl, t-butyl}

(R4b) $O(^1D)$ + isobutane $\rightarrow$ other products

A fraction of the HO produced by reactions (R3) and (R4a) subsequently absorbs photons within the same laser pulse (and in succeeding pulses if the sample flow rate is too slow). The resulting fluorescence produces an added background source which can lead to net negative interference in the detection of ambient HO. This spurious background is called resonant since it is excited only at wavelengths absorbed by HO, in contrast with the broadband excitation of other contributions to the gross background $B_1 + B_2$.

In spectral modulation of the signal from ambient HO, the behavior of I in equation (2) as ozone interference, due to reactions (R1)-(R3), has been analyzed [*Hanabusa et al.*, 1977; *Hard et al.*, 1980; *Ortgies et al.*, 1981; *Davis et al.*, 1981*a*, *b*; *Wang et al.*, 1981; *Wang and Davis*, 1982; *Shirinzadeh et al.*, 1987*a*; *Smith and Crosley*, 1990]. We have argued previously [*Hard et al.*, 1984], and maintain here, that chemical modulation is more successful than spectral modulation in excluding net interferences due to laser-produced HO.

In chemical modulation of ambient HO, *Hard et al.* [1989] noted two chemical mechanisms that lead to significant interference. These paths, and other smaller effects, are quantified here by experimental measurements and are also described by a theoretical model. The experiments are carried out in the FAGE2 instrument [*Hard et al.*, 1986] so that the results are applicable to the ambient HO measurements in that paper as well as the present ones. The purposes of the model are to (1) verify that the observed ozone interferences are consistent with the calibrated HO

response within the uncertainty of the model; (2) evaluate other possible interferences, such as H_2O_2 photolysis; and (3) predict the performance of modified instruments in terms of both interference and snr.

New measurements of rate coefficients and nascent distributions, especially those involving the isobutane reagent, can upset the apparent agreement of the model with our experimental results. Given the uncertainties in the theoretical model, disagreements of a factor of 2 or so are not consequential, since the model is not used to correct past data, but rather to identify interferences and prevent them in the design of the third-generation (FAGE3) instrument [*Chan et al.*, 1990]. Throughout this paper, resonant backgrounds and interferences are normalized to the signal from ambient HO at the given humidity.

EXPERIMENTAL CONDITIONS

Ambient HO, photochemical backgrounds, and net interferences were measured with the FAGE2 instrument, briefly described by *Hard et al.* [1986]. This instrument, installed in a converted motor home used as a field research vehicle, differed only in minor details from its previous laboratory rooftop installation [*Hard et al.*, 1986]. The instrumental parameters of FAGE2 are listed in Table 1. The 30-Hz Nd:YAG-pumped Rh6G dye laser (Quantel YG580 + TDL50) was frequency doubled and tuned to the $Q_1 1,1' + R_2 3$ line group of the $A\ ^2\Sigma\ (v'=1) \leftarrow X\ ^2\Pi\ (v''=0)$ band of HO at 282 nm. The UV laser beam was delivered to a multipass White cell via a 2-m path through two uncoated right-angle prisms, a focusing lens, and an uncoated cell window near normal incidence. (The arrangement used in the rooftop studies differed only in requiring a 7-m path and three right-angle prisms.) The linewidth of the 282-nm laser output was 0.3 cm^{-1}. The measured laser pulse shape was well described by the positive lobe of a sine wave of half-period 10 ns (Figure 2). The laser energy in the first pass through the White cell during the interference experiments was 0.6 mJ per pulse, whereas in ambient HO determinations it ranged between 0.3 and 0.6 mJ. Thus interference measurements at 0.6 mJ provide an upper limit to those present in the ambient studies; moreover, calibration before and after each ambient measurement period yields an HO response appropriate to the available laser energy during that period. (The nominal UV pulse energy of 1 mJ quoted for the rooftop system by *Hard et al.* [1986] was measured at the laser output and did not take into account all partially reflecting surfaces traversed in reaching the detection zone.) The White cell was of the asymmetric type ($4n+2$ passes, with $n=4$) [*Pickett et al.*, 1970], with mirror radii of curvature 0.5 m. To avoid damage to the mirror coating, the incoming UV beam was focused 5 cm before the entrance window and 10 cm before passing the edge of the mirror nearest the entrance of the cell, on which there were two rows of four spots each. Near the center of the cell the first-pass beam diameter was 0.6 cm, and successive passes alternated between 0.4 and 0.6 cm; there was partial overlap between some of the beams. For single-pass experiments the rear mirror-pair assembly was removed. There were two parallel sample flow channels, each fed by a separate nozzle and cylindrical flow tube. The centers of the two flow channels intersected the laser beams 3.75 cm from the center of the cell toward either end. Multipass excitation scans of the $Q_1 2,2'$ line group indicated significant radiative saturation of the absorbing transitions at an energy of 0.6 mJ. Each of the sample flows was observed by a single detection channel at right angles to the flow and to the laser propagation direction.

In each channel the sample flow (8 L/min) was provided by a 1.0-mm-diameter nozzle leading into a 4.8-cm ID cylindrical flow tube. The sample underwent choked flow

TABLE 1. Instrumental Variables and Concentrations Used in Ozone Interference Model of FAGE2 (YAG/dye 282-nm Excitation)

	Value	Notes
Total pressure in detection cell	4 torr (±1%)	*a*
O_3	50 ppb	*b*
External H_2O	0 to 20 torr	*b*
Isobutane	0 and 575 ppm	*a*
Beam diameter, first and odd laser passes	0.6 cm (±10%)	*a*
Beam diameter, second and even laser passes	0.4 cm (±10%)	*a*
Pulse energy	0.6 mJ (±10%)	*a*
Pulse shape	sine wave	*c*
Pulse duration	6.67-ns FWHM, 10-ns base width (±5%)	*a*
Laser linewidth	0.3 cm^{-1} (±10%)	*a*
Ambient HO chemical loss during sampling	2%	*d*
Ambient HO chemical modulation efficiency	95% (±2%)	*a*
Detection gate, relative to start of laser pulse	110 ns to 360 ns	*a*
Multipass/single-pass ratios		
ambient HO response	8.0 (±1.0)	*a*
resonant background normalized to ambient HO response	7.5 (±1.0)	*a*

Quoted uncertainties are 1σ estimates.

[a] Measured.

[b] Assumed for modeling purposes.

[c] Approximation to measured shape.

[d] Value which gives agreement between interference experimental data and model.

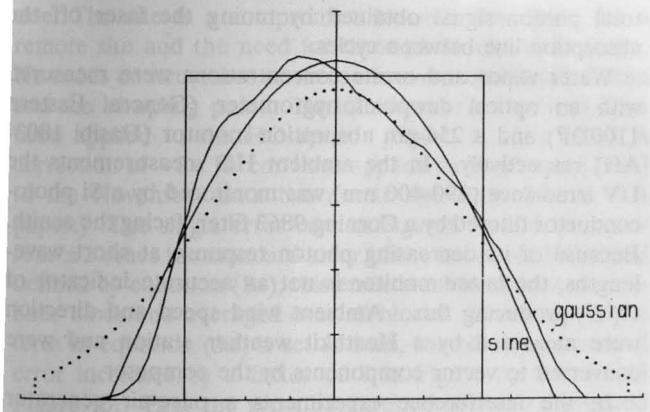

Fig. 2. Measured YAG/dye waveform, with superimposed squarewave, half-sinewave, and truncated Gaussian, all with same FWHM and area.

through the nozzle throat, supersonic expansion, deceleration within the rapidly expanding concave diffuser, and subsonic flow down the remainder of the nozzle exit and the tube. Although conditions for laminar flow were satisfied, flow modeling [*Migliore and Bishop*, 1988], using a computational grid extending 11 cm downstream from the nozzle and a velocity vector plot extending to 6 cm for the present case, indicates a central jet for at least the first 6 cm and flow that is neither parabolic nor plug flow. The distance between the nozzle and the fluorescence detection zone was 35 cm and the calculated plug-flow velocity was 1400 cm/s, so that 25 ms represents a computed plug-flow transit time for the air sample. A central portion of the flow was viewed by the fluorescence detector; thus the value of the transit time was between the values for plug flow (25 ms) and for the central maximum of parabolic flow (12.5 ms). At the detection zones, four large holes in the flow tube walls at 90° intervals permitted passage of the laser beams and collection of the HO fluorescence and backgrounds. Contrary to an incorrect impression that readers of *Smith and Crosley* [1990] may have obtained from the schematic diagram in their Figure 2, there were no windows in the flow tube walls along the laser excitation axis, and the flow tubes' diameter remained constant until they emptied into a common manifold several centimeters below the detection zone. After leaving the manifold the flow passed through an adjustable restricting valve to a 300 cfm Roots-type pumping system, which allowed maintenance of cell pressure at 4 torr. Although there was no window separating the two channels in the cell, cross flow was minimized by symmetric design of the two flow paths into the large manifold. The extent of cross flow was measured by placing a source of high concentration HO at one nozzle and monitoring HO fluorescence at the other observation region, and vice versa; the resulting cross talk between the two channels was less than 1%.

The interior of the nozzles and the first 30 cm of the cylindrical flow tubes leading to the detection zones were coated with halocarbon wax. Table 1 lists an approximate value of 2% for the loss of ambient HO in this sampling arrangement; this value was determined by requiring agreement between experimentally observed and model-predicted values of resonant background and thus incorporates any errors in the model's input parameters. Thus the actual value of the loss may differ. For comparison, in a 50-mm ID flow tube coated with halocarbon wax, *Keyser* [1981] observed an HO wall loss rate of ~5 s^{-1}. This would correspond to approximately 12% loss at the plug-flow transit time of 25 ms in the present flow tube. Any HO sampling loss is present during both ambient HO measurement and calibration and therefore is not used in calculating ambient HO concentrations. Diurnal variation of the loss is possible; however, we have done short-term experiments, using an external constant-temperature HO source while varying the temperature of the nozzle head and tube over a range greater than ambient, and have found negligible (less than 10%) HO signal variation with temperature. Moreover, even during the calibration procedure [*Hard et al.*, 1984, 1986] in which the interior and exterior walls of the HO probe were exposed to varying concentrations of the oxidation products of 1,3,5-trimethylbenzene, no change in HO response with time was noted (R. J. O'Brien et al., Rapid response HO measurements and hydrocarbon reactivity, submitted to *Journal of Atmospheric Chemistry*, 1990).

About 5-mm downstream from the entrance of each nozzle, three small inlets at 120° intervals, flush with the interior wall and connected via a low-volume manifold, admitted 200 mL/min of carrier gas (air in these experiments) to the 8 L/min main flow. A controlled flow of isobutane (Matheson instrument grade, 99.5%), which was used to modulate ambient HO by chemical removal [*Hard et al.*, 1984, 1986], was added to the carrier gas when appropriate. Calibration of the flow controller gave a value of 575 ppm for the standard isobutane concentration relative to the total sample and carrier flow, 25% greater than the previously reported value [*Hard et al.*, 1989], which was based on the manufacturer's N_2 calibration and recommended conversion factor for isobutane. The measured chemical modulation, (95±2)%, yielded an effective transit time of 16 ms (±25%, based upon uncertainty in the reaction rate constant) for the portion of the flow intersecting the detector field of view. This indicates that the overall flow may be closer to parabolic, which would yield a transit time of 12.5 ms, 1/2 the plug-flow velocity.

In each channel, fluorescence in the $A\ (v'=0) \rightarrow X\ (v''=0)$ band was collected at f/1.5, filtered by a multilayer interference filter (309-nm effective center wavelength, 3-nm full width at half maximum (FWHM) passband), and focused on a mask in front of a 14-stage bialkali photomultiplier (EMI 9813QKB). The mask limited the observed laser beam length to 2.0 cm. A concave mirror opposite the collecting lens, with its radius of curvature centered on each detection zone, served to increase the detected signal by a factor of about 1.5. In normal operation the outputs from the photomultipliers were fed without further amplification to the gated charge-integrating inputs of LeCroy 3001qVt multichannel analyzers (MCA), which digitized the anode-charge signals on each laser pulse. The gate, triggered by the laser via a photoconductive diode, began 110 ns after the leading edge of the detected signal from the first passage of the laser pulse through the HO detection zones and ended 250 ns later. A home-built interface transmitted the signals to a computer for processing and storage, with real-time averaging and plotting. The computer also controlled the valves which directed isobutane to alternating channels, and stored ozone and water concentration, laser power, and spectral overlap data.

To provide absolute photon signals for use with equation (4*b*), we used two methods to measure the numerical factor for conversion of photoelectrons to pulsed anode charge in each photomultiplier tube (PMT). Both methods used attenuated continuous light to provide low photon arrival rates, to insure that double photon values were rare, verified with the aid of a 400-MHz oscilloscope connected to the anode of either PMT. One method used the oscilloscope, self-triggered at the lowest threshold voltage which allowed the trace to be fully extinguished when the light source was turned off. With the light source on, the resulting multiple trace showed a vertical distribution of peak voltages; the trace of maximum brightness was taken to be the average pulse, whose area was converted to a pulse charge using the total input impedance. This charge was then multiplied by the multichannel analyzer's stated conversion factor for analog charge to the digital values that were transmitted to the computer. The second method did not require the use of the latter factor, since each MCA provided a display of the distribution of event frequency versus gated charge. By laser-triggering the MCA, while detecting the attenuated continuous light source, photon arrival rates much less than 1 per gate interval were obtained. The most frequent value of gated charge, minus a pedestal value corresponding to zero charge, was taken as the average value of digitized charge per photon. The results of the two methods agreed to within 25%.

The standard measurement cycle employed the chemical-modulation method used in ambient HO determination [*Hard et al.*, 1986], with minor modifications. The cycle consisted of eight intervals of 200 laser shots, each preceded by a 2-s pause for the switched reagent to reach steady concentration in the low-pressure sample flow. Data processing at the end of the eighth interval brought the full cycle length to 70 s. The "square wave" of reagent flow reversed phase at the middle and the end of the cycle (Table 2) to minimize net effects of drift in laser power and atmospheric background fluorescent species concentrations. In ambient measurements and in interference studies the power and spectral overlap of the laser with the HO absorption were monitored and were manually adjusted as necessary. The spectral overlap was measured in a separate cell (source 2 in the work by *Hard et al.* [1984]), excited by the same laser beam, yielding HO fluorescence signals sufficiently strong that the resulting waveforms were observed on an analog oscilloscope; this permitted laser wavelength tuning when necessary. In the interference studies the gross HO-resonant background was measured by taking the change in total photon signal obtained by tuning the laser off the absorption line between cycles.

TABLE 2. Reagent Modulation Cycle Used in Measurement of Ambient HO

	Channel 1	Channel 2
1	off ($S+B_1$)	on (B_2)
2	on (B_2)	off ($S+B_1$)
3	off	on
4	on	off
5	on	off
6	off	on
7	on	off
8	off	on

Water vapor and ozone concentrations were measured with an optical dewpoint hygrometer (General Eastern 1100DP) and a 254-nm absorption monitor (Dasibi 1003-AH) respectively. In the ambient HO measurements the UV irradiance (290-400 nm) was monitored by a Si photoconductor filtered by a Corning 9863 filter, facing the zenith. Because of its decreasing photon response at short wavelengths, the latter monitor is not an accurate indicator of $O(^1D)$-producing flux. Ambient wind speed and direction were measured by a Heathkit weather station and were converted to vector components by the computer.

In the interference experiments a pure-air generator (AADCO 20 L/min) supplied an excess flow of air to both sampling nozzles, via a symmetrically forked delivery tube with two outlets. Loose-fitting contact between each of the latter outlets and the respective nozzles allowed the excess flow to escape, avoiding changes in flow through the nozzles caused by varying excess pressure. Water vapor was added by bubbling a fraction of the air through liquid water in a thermostatted container. Spray droplets were trapped by passing the moist air through two flasks serving as impactors. Ozone at concentrations below 1ppm was supplied by a continuous flow of cylinder O_2 past a low-pressure quartz Hg pen-ray lamp, followed by a flask containing stainless-steel wool to remove free radicals, before mixing with the main pure-air flow. Water vapor and ozone concentrations were continuously sampled upstream from the delivery fork, and measured as above.

Fluorescence waveforms, required for measurement of rate constants for HO quenching by isobutane, were measured by connecting one channel's photomultiplier output to a 400-Mhz analog oscilloscope (Tektronix 2467B) and digitizing the resulting CRT traces with an array camera, computer plug-in card, and associated waveform averaging software (Tektronix DCS01). Transient PMT saturation by space-charge effects in the PMT's internal amplifying chain was detected by comparison of derived logarithmic-decay slopes at varying peak photon-signal inputs; the decay rate coefficients presented below were obtained by fitting the time region where PMT saturation effects were found to be not significant. Photolysis of O_3+H_2O mixtures provided the necessary HO source on a time scale short enough to prevent the chemical removal of groundstate HO by isobutane. Each reported waveform is the net difference between averages of 1500 to 5000 traces taken on and off the HO absorption line. Further description of the waveform measurement and its uncertainties is given below.

EXPERIMENTAL RESULTS

Ambient Data

Examples of ambient HO measurements at our Oregon coastal site (45°N 124°W) are shown in Figure 1, with 1-hour running averages as in our previously reported measurement in June 1985 [*Hard et al.*, 1986]. In contrast with the 1985 data, here continuous ozone measurements were obtained, which allow an investigation of the apparent dependence of signal and offsets on ozone concentration. The site is in Lincoln City, Oregon, with the HO sampling point 8 m horizontally and 5 m vertically from mean high

tide. The site is a compromise between the desire for a remote site and the need for three-phase electrical power. No roads or structures intervene between the Pacific Ocean and the sampling point. No interference corrections have been applied to the HO data in Figure 1. (As noted, a correction of -2×10^5 cm^{-3} was applied by *Hard et al.* [1986] to the November data but not to the June data in that paper.) The single error bars in Figures 1*a* and 1*b* represent ±2 times the standard error of the mean net HO signal defined by equation (3*a*); this error is calculated for each 1-hour block and averaged over all blocks. If the covariance term in equation (3*a*) is set to zero, the resulting standard error increases by a factor of 8 in Figure 1*a* and 6.5 in Figure 1*b*. Thus the gross background is highly correlated within the modulation cycle, which is not surprising since nearly all of the background comes from scattering and fluorescence of laser radiation by air and by cell components. Supporting data on other ambient variables are also provided; however, water vapor is missing in Figure 1*b* because of malfunction of the dewpoint hygrometer.

In Figure 1*a*, H_2O is essentially constant at approximately 10 torr; a seaward-landward wind cycle appears to be present, leading to nocturnal ozone removal by surface deposition and local combustion-produced NO_x. At 18 hours on May 5 and May 6, HO declines with daylight to low nighttime values at least 3 hours before ozone does; this observation can be taken as independent evidence for an ambient HO signal greater than any positive or negative offset due to ozone interference. Before twilight on May 6, the signal averages about -3×10^5 HO cm^{-3} in the absence of ozone. During August 18-20, 1987 (Figure 1*b*), ozone persists through both nights, and greater negative nighttime offsets are apparent than in Figure 1*a*. During both measurement periods, nighttime fluctuations in signal with amplitude of several times 10^5 cm^{-3} and period of several hours are present.

In Figure 1*a* the May 6 midafternoon drop in HO begins at the same time as a 50% decline in ozone and persists after the ozone concentration returns to its previous value. Reasons for the drop in ozone concentration and the subsequent failure of HO to follow ozone's recovery are not obvious. In both Figures 1*a* and 1*b*, HO follows ambient UV more closely than it follows ozone.

Hydrocarbon grab samples were taken at 1440 on May 5, 1615 on May 6, and 1530 on August 19, using evacuated containers kindly supplied and subsequently analyzed by James Greenberg and coworkers of the National Center for Atmospheric Research. The four samples yielded total nonmethane hydrocarbon concentrations of 32, 43, and 25 ppbvC (carbon atoms), and total C_2 + C_3 alkane + alkene concentrations of 4.6, 3.7, and 3.4 ppbv (compound), respectively. In all four samples, either C_3H_8 or the sum of n-C_4H_{10} and i-C_4H_{10} was greater than C_2H_6, suggesting a possible contribution from the kitchen stoves of a motel 30 m due north. The C_2 + C_3 totals are less than 5 times those reported by *Carroll et al.* [1990] for the marine boundary layer at approximately 0.2 km altitude on GTE/CITE 2 Flights 7 and 10 off the Southern California coast, August 19 and 26, 1986. At the same altitude Carroll et al. found typical NO_x concentrations of 8 to 30 ppt. Under the unproven assumption that NO_x concentrations are proportional to NMHC in the marine boundary layer, we estimate an NO_x range of 25 to 135 ppt at our NMHC sampling times. The low total NMHC concentrations imply remote-air conditions for sea-level tropospheric air, at least at these sampling times, despite the apparent presence of a local source of excess C_2 and C_3 hydrocarbons. In Figure 1*b* a further indication of remote-air conditions is the persistence of ozone at night. In both Figures 1*a* and 1*b*, ozone appears to decline with decreasing wind velocity, suggesting that its persistence at night in Figure 1*b* is maintained by vertical mixing, which is stronger in the presence of surface winds.

Figure 3 shows the sums of the distributions of the net HO signal rates M_i within each hour about the hourly means M of the HO data of Figures 1*a* and 1*b*. The data belong to normal distributions, and thus the calculation of average 2σ error bars is justified.

In Figure 4 the ambient HO data of Figures 1*a* and 1*b* are replotted with the minimum averaging times necessary to reach snr ≥ 5. The width of each block is its required averaging time. In contrast with the moving HO averages of Figure 1, each net HO datum contributes to only one block average in Figure 4. HO data are accumulated until the snr ($= M/e_M$, with e_M defined by equation (3*a*) or (3*b*)) of the mean net HO signal rate M has reached a value of at least 5, and then a new average begins with the next raw HO datum. To avoid undesirable skewing of the daytime data with respect to time, averaging starts with each day's peak HO signal and moves first toward earlier times, stopping at the preceding midnight, and then starts a new average in the forward direction beginning with the datum immediately following the peak, stopping at the following midnight. The number above each block that crosses midnight is the snr (< 5) of the sum of the unused data remaining on both sides of midnight. Figure 4 shows that the daytime positive HO signals in Figure 1 are more significant than the negative offsets detected when ambient HO is lower or absent.

To date, the variation of ambient [HO] with time of day has been measured by at least four independent methods. Table 3 lists recent experimental observations of peak

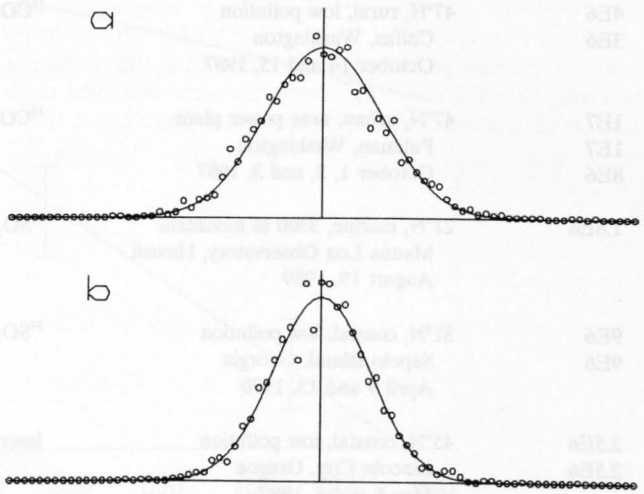

Fig. 3. Sums of distributions of net HO signals in each hour about their hourly means. Solid curves are Gaussians, demonstrating that the net signals belong to a normal distribution: (*a*) May 5-7, 1987; (*b*) August 18-20, 1987.

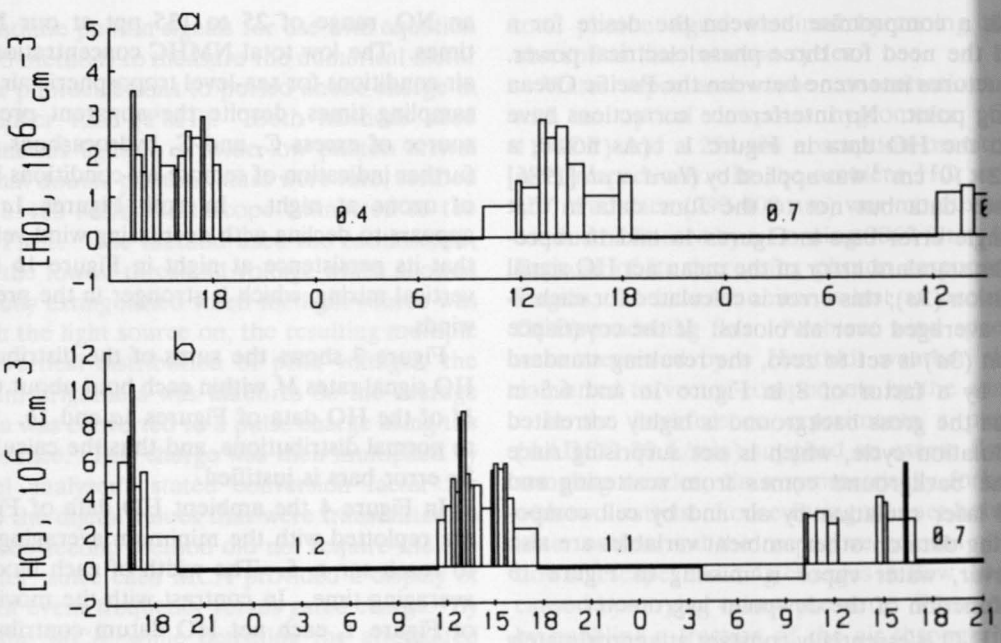

Fig. 4. Ambient HO signals averaged to snr ≥ 5, with e_M calculated from equation (3*b*). Averaging begins at each day's peak, runs to the previous midnight and then to the following midnight. The data adjacent to each midnight that do not reach snr = 5 are summed, and the numeral above the resulting bar gives the corresponding snr: (*a*) May 5-7, 1987; (*b*) August 18-20, 1987.

TABLE 3. Experimental Observations of Peak Daytime [HO]

[HO]	Conditions	Method	Reference
6E6[a]	48°N, rural, 1220 m mountain Black Forest, Germany June 25, 1984	long-path UV laser absorption	*Platt et al.* [1988]
3.5E6	45°N, urban, low pollution Portland, Oregon June 18, 1985	laser-excited low-pressure fluorescence	*Hard et al.* [1986]
1.5E6	42°N, urban Dearborn, Michigan July 15, 1986	laser-excited low-pressure fluorescence	*Shirinzadeh et al.* [1987*b*]
4E6 3E6	47°N, rural, low pollution Colfax, Washington October 14 and 15, 1987	$^{14}CO \rightarrow {}^{14}CO_2$, cryoseparation, counting	*Felton et al.* [1988]
1E7 1E7 8E6	47°N, urban, near power plant Pullman, Washington October 1, 2, and 3, 1987	$^{14}CO \rightarrow {}^{14}CO_2$, cryoseparation, counting	*Felton et al.* [1988]
1.8E6	21°N, marine, 3300 m mountain Mauna Loa Observatory, Hawaii August 19, 1989	$^{34}SO_2 \rightarrow \rightarrow {}^{34}HSO_4^-$, mass spectrometry	*Eisele and Tanner* [1991]
9E6 9E6	31°N, coastal, low pollution Sapelo Island, Georgia April 9 and 13, 1990	$^{34}SO_2 \rightarrow \rightarrow {}^{34}HSO_4^-$, mass spectrometry	*Eisele and Tanner* [1991]
2.5E6 2.5E6	45°N, coastal, low pollution Lincoln City, Oregon May 5 and 6, 1987	laser-excited low-pressure fluorescence	present work
8E6 6E6 3E6	45°N, coastal, low pollution Lincoln City, Oregon August 18, 19, and 20, 1987	laser-excited low-pressure fluorescence	present work

[a] Read 6E6 as 6×10^6 cm^{-3}.

daytime [HO] for comparison. Earlier observations have been summarized by *Hewitt and Harrison* [1984] and *Altshuller* [1989]. Comparisons among the experimental results in Table 3 are hindered by insufficient simultaneous measurements of the principal trace species that influence [HO]. In remote air, at the very least, O_3, CO, and NO measurements would be desirable for such comparisons to be meaningful. However, the present observed peak [HO] results are within a range defined by the results of three other independent techniques: long-path UV laser absorption [*Platt et al.* 1988], radiochemical measurement of ^{14}CO oxidation to $^{14}CO_2$ [*Felton et al.*, 1988], and conversion of $^{34}SO_2$ to $H^{34}SO_4$ with mass spectrometric detection [*Eisele and Tanner*, 1991].

Photochemical Interference Results

Excitation spectral scans of the *A* $(v'=1) \leftarrow X$ $(v''=0)$ band in the presence of ozone and water vapor, in which each laser pulse serves as both the photolysis source of $O(^1D)$ and the HO probe, indicate the presence of rotationally hot groundstate HO, in qualitative agreement with previous studies [*Comes et al.*, 1981; *Gericke and Comes*, 1980, 1982; *Gericke et al.*, 1981; *Butler et al.*, 1981; *Rodgers et al.*, 1981; *Cleveland*, 1988]. In contrast, in dry air with ozone and isobutane, excitation scans indicate a near-equilibrium groundstate rotational distribution, as would be expected from an earlier study of the reactions of $O(^1D)$ with other C_3-C_5 alkanes [*Luntz*, 1980].

We have carried out a quantitative assessment of the negative offsets present in ambient data such as those in Figure 1. To do this we have systematically varied O_3, H_2O, and isobutane in pure air delivered to the FAGE2 instrument as described above. We find small negative offsets consistent with the ambient data, as described next.

At the $Q_1 1,1' + R_2 3$ line, using the chemical-modulation system designed for ambient HO determination, we observed the dependence of interference on $[O_3]$ in dry air at three isobutane concentrations, shown in Figure 5. The data closest to zero net signal correspond to the "standard" isobutane concentration (7.5×10^{13} molecules cm^{-3} at 4 torr) used to modulate ambient HO in the work by *Hard et al.* [1986], as well as in the ambient measurements reported here. The O_3+isobutane photochemical interference was negative (with respect to ambient HO) because it increased the total background during the part of the cycle normally devoted to background measurement (equation (2)), chiefly through reaction (R4*a*).

In moist air, at a constant O_3 mole fraction of 50 ppb, we measured the net interference as a function of H_2O external vapor pressure at four isobutane concentrations, with the results shown in Figure 6. As above, the points closest to zero net signal correspond to the standard isobutane concentration. The effect of H_2O is to reduce the magnitude of the negative interference somewhat from its value in dry air, for reasons discussed below. Nevertheless, the sum of all ozone interferences is negative over the range of ambient humidities.

Besides the net HO-resonant interferences obtained by chemical modulation with isobutane and shown in Figures 5 and 6, we also measured the gross HO-resonant background (Figure 7) by spectral modulation during the above experiments. This background, $B_1 + B_2$, is the sum of the signals (due to HO from reactions (R3) and (R4*a*)) collected from the two channels. In dry air the gross resonant backgrounds were approximately equal to the absolute values of the net interferences shown in Figure 5. In contrast, moist air produced the much larger HO-resonant backgrounds displayed in Figure 7. These are "backgrounds" with respect to chemical modulation of ambient HO, but "interferences" if spectral modulation is used for ambient HO measure-

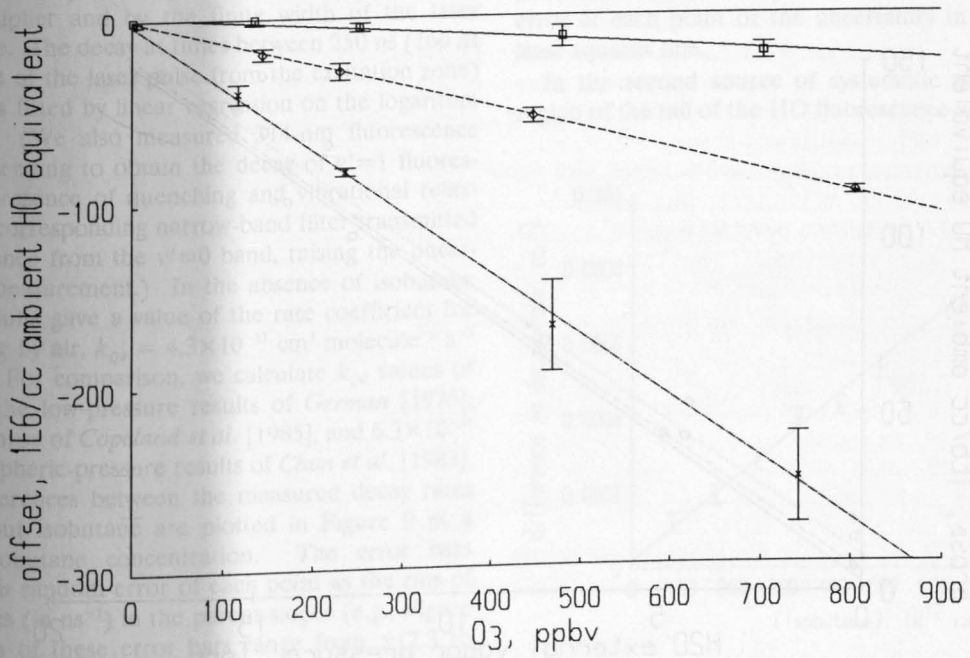

Fig. 5. Net interference versus ozone concentration in dry air, at three isobutane concentrations in FAGE2 instrument. Open squares: standard [*i*-BuH]; open diamonds: 5× standard; and crosses: 12.5× standard. Error bars represent $\pm 1\sigma$ uncertainties of the mean interference at the respective points. Straight lines are least squares fits to the experimental data.

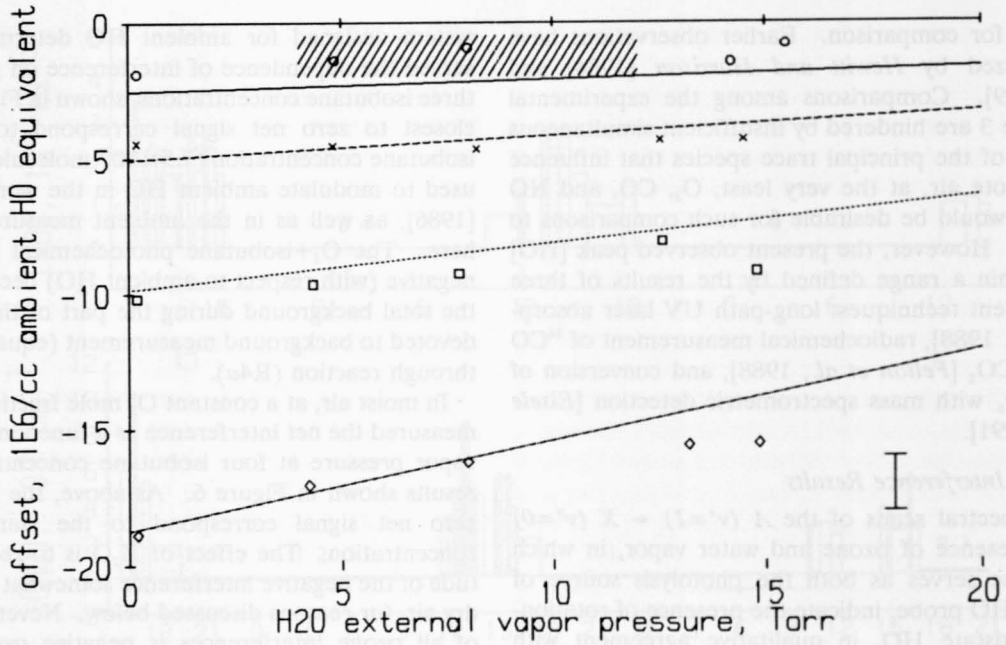

Fig. 6. Net interference versus H_2O ambient partial pressure, at O_3=50 ppb and four isobutane concentrations in FAGE2 instrument. Open circles and solid lines: standard [i-BuH]; crosses and dashed lines: 2× standard; open squares and dotted lines: 4× standard; open diamonds and dashed-dotted lines, 8× standard. Error bar represents $\pm 1\sigma$ uncertainties averaged over all points. Straight lines are derived from model described in text. Shaded box corresponds to instrumental conditions appropriate to data of Figure 1. At 50 ppb ozone the experimentally determined negative offset is about -1.5×10^6 cm^{-3}, and is weakly dependent upon water vapor concentration.

ments. When photochemical HO production by the laser is significant, it is clear from comparison of Figures 6 and 7 that chemical modulation is superior.

All of the above results were obtained with multipass excitation, as in our ambient measurements. Single-pass results, obtained by removing the multipass mirrors from the cell, yielded a multipass-to-single-pass ratio of 8.0 ± 1 for the responses to external HO. A similar measurement of gross resonant backgrounds (B_1 + B_2), expressed in units of the respective HO responses, yielded a multipass-to-single-pass ratio of 7.5 ± 1. At the typical ambient conditions of Figures 1*a* and 1*b* (30 ppb O_3 and 10 torr H_2O) the magnitude of the negative offset calculated from Figure 6, -1.3×10^6 HO cm^{-3}, is in rough agreement with the offset observed in Figure 1*b*, taking into account the noise present in the ambient measurement. Note also that the laser

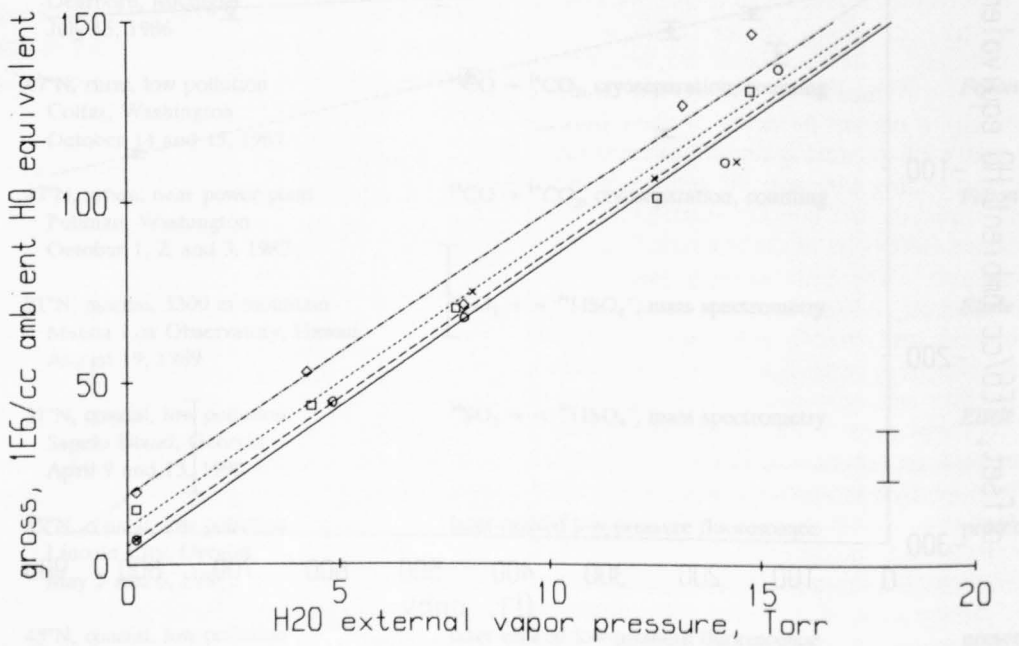

Fig. 7. Gross HO-resonant background versus H_2O ambient partial pressure. Symbols same as in Figure 6. Straight lines are derived from model described in text.

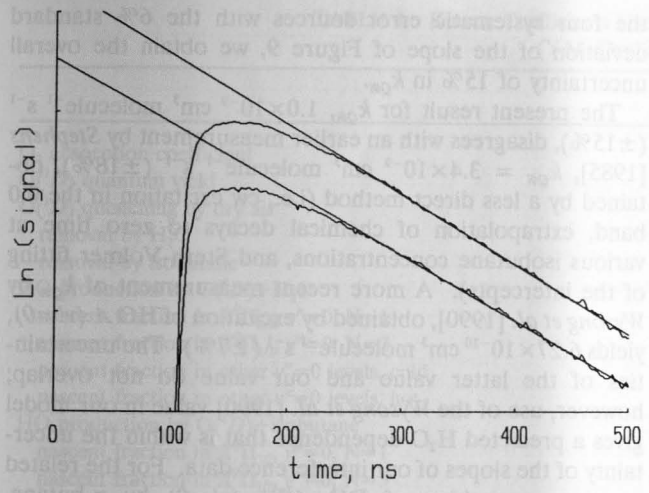

Fig. 8. HO 309-nm logarithmic decay waveforms. HO was generated by 282 nm laser photolysis of O_3 in the presence of H_2O. Upper curve: with isobutane; lower curve, without isobutane; straight lines: least squares fits between 250 and 500 ns on indicated scale.

energy used in measuring interferences in Figure 6 was 0.6 mJ per pulse, compared with a range of 0.3 to 0.6 mJ during the ambient HO measurements of Figure 1*b*.

A reliable value of k_{Q0i}, the HO A $(v'=0)$ + isobutane quenching rate coefficient, is necessary for the prediction of the positive component of the net interference. In order to measure k_{Q0i} the 309-nm fluorescence waveforms of the ozone-produced interferences were obtained, with and without isobutane, with multipass and single-pass excitation, at an H_2O partial pressure of 6 ± 0.6 torr before expansion. Sample waveforms are shown in Figure 8. The rising portion of the waveform is due to the decay of the A $(v'=0)$ state, via vibrational relaxation to the observed A $(v'=0)$ state and quenching to the X state. The shape of the rising portion is distorted by recovery from transient saturation of the photomultiplier and by the finite width of the laser excitation pulse. The decay at times between 250 ns (160 ns after departure of the laser pulse from the excitation zone) and 500 ns was fitted by linear regression on the logarithm of the signal. (We also measured 314-nm fluorescence waveforms, intending to obtain the decay of $v'=1$ fluorescence in the presence of quenching and vibrational relaxation, but the corresponding narrow-band filter transmitted some fluorescence from the $v'=0$ band, raising the uncertainty of this measurement.) In the absence of isobutane the 309-nm results gave a value of the rate coefficient for $v'=0$ quenching by air, $k_{Q0} = 4.3\times10^{-11}$ cm^3 molecule^{-1} s^{-1} (1σ = ±5%). For comparison, we calculate k_{Q0} values of 4×10^{-11} from the low-pressure results of *German* [1976], 5×10^{-11} from those of *Copeland et al.* [1985], and 6.3×10^{-11} from the atmospheric-pressure results of *Chan et al.* [1983].

The net differences between the measured decay rates with and without isobutane are plotted in Figure 9 as a function of isobutane concentration. The error bars represent the 1σ random error of each point as the rms of the uncertainties (in ns^{-1}) in the parent slopes (e.g., Figure 8). The values of these error bars range from ±(2.3 to 3.1)$\times10^{-5}$ ns^{-1}. The rate coefficient for relaxation of HO $A^2\Sigma^+$ $(v'=0)$ by isobutane, derived from the slope of the least squares fit of the data in Figure 9, is $k_{Q0i} = 1.0\times10^{-9}$ cm^3 molecule^{-1} s^{-1} (±15%). This result is measured absolutely, without reference to the quoted result for quenching by air. The standard deviation of the slope in Figure 9 is only 6% of k_{Q0i}; however, the estimated 15% uncertainty in k_{Q0i} includes possible systematic errors.

Four sources of systematic error are considered. The first involves the accuracy of waveform excitation and measurement, the second arises from the difference-of-exponentials nature of the waveform, the third is introduced by taking the logarithms of waveforms that contain noise, and the fourth concerns the isobutane concentration in the flow tube. Regarding the first source, each pixel of the two-dimensional array of the digitizing camera has an eight-bit gray scale; the camera system uses this information to interpolate to the center of the trace thickness. For the latter interpolation, combined with this oscilloscope's vertical noise and this camera's readout noise, the manufacturer has measured an effective vertical resolution of 9.5 bits for single waveform acquisition; averaging of such waveforms in the six-digit floating point memory allows effective 12-bit resolution to be achieved. The latter result is independent of the chosen time display pitch, as long as the trace brightness is in an acceptable range, easily determined at the start of the experiment. The scope's CRT and camera geometric distortions are removed by a calibration procedure in which the camera hardware supplies dc levels and waveforms of known frequency to the scope and uses the results to correct subsequent experimental waveforms. The analog scope's risetime (=decay time) is 0.35/400 MHz = 0.875 ns. The decay time without isobutane is 175 ns, and at the maximum isobutane used it is 150 ns. Using $\tau_{meas} = (\tau_{real}^2 + \tau_{instr}^2)^{1/2}$, the resulting relative errors in the latter decay times are 1.25×10^{-5} and 1.7×10^{-5}; the resulting relative error in the net decay due to isobutane is -3×10^{-5}. A larger error arises from multipass excitation; assuming 20-ns FWHM for the effective pulse width, a similar calculation results in a relative error of −1.6% in the net decay rate at the highest isobutane concentration; this is less than either the random error at each point or the uncertainty in the slope of the least squares line.

In the second source of systematic error the sampled region of the tail of the HO fluorescence waveform contains

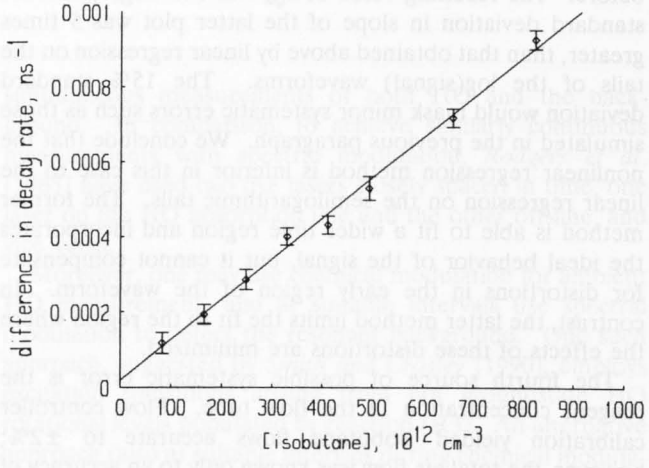

Fig. 9. Difference in HO 309-nm decay rate versus isobutane concentration, used to obtain quenching rate coefficient for $A^2\Sigma^+$, $v=0$ by isobutane. Straight line is least squares fit to experimental data.

a small contribution, decreasing with time, from the decay processes occuring during the rising region. At the start of the fitted region this contribution is between 1% and 2% of the instantaneous signal, depending on the values of the total decay rates of $A\ (v'=1)$ and $A\ (v'=0)$. In the absence of noise in the waveforms the resulting relative error in the fitted slopes is between −0.6% and −0.7%. The error in the difference between the fitted slopes (yielding k_{Q0i}) is proportional to the concentration of the modulating reagent and is between −0.7% and −1.2% at the highest isobutane concentration used.

To estimate the effects of the third source, time-varying random noise (whose amplitude is several times greater than that observed in the respective sums of raw experimental waveforms) is added to the latter simulation. In this case, 25 model runs give a population standard deviation of 18% and a systematic error (with respect to the noise-free asymptote of the decay) of −9%. Each of the first three systematic errors, if present, would lead to negative curvature of the difference data, which is not observed in Figure 9, and would lead to underestimation of the value of the quenching rate coefficient.

To evaluate the effects of the second and third error sources further, we fitted the difference-of-exponentials function $a(\exp(-k_1(t-t_0))-\exp(-k_2(t-t_0)))/(k_2-k_1)$ to the experimental signal waveforms, using Nelder-Mead simplex nonlinear regression to obtain values for a, k_1, k_2, and t_0. Since the value of this function is unchanged by an interchange of the values of k_1 and k_2, this fitting method yields k_{Q0} only as the lesser of k_1 or k_2; the greater of k_1 and k_2 ideally corresponds with the decay of the $A\ (v'=1)$ state and is associated principally with the rising portion of the waveform. Compared with linear regression on the tail region of the waveforms, the four-parameter nonlinear regression enables fitting over a wider time range, does not involve taking the logarithm of the signal, and thus may reveal systematic errors in the former method. However, the above mentioned distortion of the rising portions of the experimental waveforms leads to unreliable values for t_0 and the $A\ (v'=1)$ decay coefficient. Nonetheless we tried the four-parameter regression on the experimental waveforms over the range from 116 to 500 ns on the abscissa of Figure 8, and plotted the differences in k_{Q0} against isobutane as before. The resulting value of k_{Q0i} was 3% larger, and the standard deviation in slope of the latter plot was 5 times greater, than that obtained above by linear regression on the tails of the log(signal) waveforms. The 15% standard deviation would mask minor systematic errors such as those simulated in the previous paragraph. We conclude that the nonlinear regression method is inferior in this case to the linear regression on the semilogarithmic tails. The former method is able to fit a wider time region and incorporates the ideal behavior of the signal, but it cannot compensate for distortions in the early region of the waveform. In contrast, the latter method limits the fit to the region where the effects of these distortions are minimized.

The fourth source of possible systematic error is the reagent concentration in the flow tube. Flow controller calibration yielded isobutane flows accurate to ±2%; however, the total air flow was known only to an accuracy of ±10% and the pressure to ±3%. Thus the uncertainty in k_{Q0i} due to systematic errors of unknown sign in the isobutane concentration is ±10%. Combining the estimates of the four systematic error sources with the 6% standard deviation of the slope of Figure 9, we obtain the overall uncertainty of 15% in k_{Q0i}.

The present result for k_{Q0i}, 1.0×10^{-9} cm^3 molecule^{-1} s^{-1} (±15%), disagrees with an earlier measurement by *Stephens* [1985], $k_{Q0i} = 3.4\times10^{-9}$ cm^3 molecule^{-1} s^{-1} (±18%), obtained by a less direct method (i.e., cw excitation in the 0,0 band, extrapolation of chemical decays to zero time at various isobutane concentrations, and Stern-Volmer fitting of the intercepts). A more recent measurement of k_{Q0i} by *Wysong et al.* [1990], obtained by excitation of HO $A\ (v'=0)$, yields 6.27×10^{-10} cm^3 molecule^{-1} s^{-1} (±7%). The uncertainties of the latter value and our value do not overlap; however, use of the *Wysong et al.* [1990] value in our model gives a predicted H_2O dependence that is within the uncertainty of the slopes of our interference data. For the related reaction, quenching of DO $A^2\Sigma^+$ $(v'=0)$ by *n*-butane, *Vaghjiani and Ravishankara* [1987] measured a rate coefficient of 9.2×10^{-10} cm^3 molecule^{-1} s^{-1} (±11%).

Discussion of Interference Data

During the moist-air experiments, H_2O and O_3 were present in both channels; thus all net interferences were introduced by the alternating addition of isobutane to either channel during the measurement cycle. Four possible effects can be distinguished, affecting B_1, B_2, and I in equations (1) and (2).

1. In the absence of isobutane, an HO-resonant background $B_1 = B_2$ is present in each channel, due to reaction of $O(^1D)$ with H_2O (reaction R3). This background is removed in the subtraction which produces the net HO signal. It does contribute to the overall noise in the measurement, and hence it affects the instrumental sensitivity, but its measured contribution to the noise is smaller than such processes as broadband air and wall fluorescence and scattering. The remaining three interferences are due to perturbation of this HO-resonant background by the addition of isobutane to the background channel.

2. Isobutane competes with M and H_2O for the available $O(^1D)$ (reactions (R2)-(R4*a*)), reducing production of HO by reaction (R3), making $B_2 < B_1$ and producing a positive offset. This offset was overestimated 1000-fold by *Shirinzadeh et al.* [1987*a*], as we have shown previously [*Hard et al.*, 1989]. The modeling reported below confirms that this effect is negligible under our low-pressure short-pulse conditions.

3. Isobutane increases the total electronic quenching rate of spurious HO, leading to $B_2 < B_1$. In ozone interference at low pressure this quenching produces a positive offset which is always smaller than the following negative offset.

4. The reaction of $O(^1D)$ with isobutane (R4a) produces additional HO, giving $B_2 > B_1$, and producing the largest offset, a negative one.

Effect 4 is dominant in creating the negative offset observed in ambient measurements and plainly accounts for the negative intercepts of Figure 6. Furthermore, although the quantitative behavior of these processes is not simple, their net result is easily measured experimentally. For example, such an empirical measurement is illustrated by the shaded box in Figure 6 which represents the range of $[H_2O]$, and an upper limit to $[O_3]$, encountered in ambient HO measurements at the isobutane concentration used to modulate the HO signal. Thus the experimentally measured

TABLE 4. Kinetic Coefficients Used in Ozone Interference Model of FAGE2 (YAG/Dye 282-nm Excitation)

	Value			Notes
O_3 absorption coefficient	3.28E−18 cm^2			*a*
$O(^1D)$ quantum yield	0.9			*b*
$O(^1D)$ quenching by dry air	2.88E−11 $molecule^{-1}cm^3s^{-1}$			*b*
removal by H_2O	2.2E−10			*b*
removal by isobutane	7.3E−10			*c*
HO production by $O(^1D)+H_2O$	2 × 2.2E−10			*b*
nascent fraction in $X^2\Pi_{3/2}$, $v''=0$, N=1	0.036			*d*
nascent fraction in $X^2\Pi_{1/2}$, $v''=0$, N=3	0.018			*d*
nascent fraction in other $v''=0$ levels, cold	0.106			*d*
nascent fraction in other $v''=0$ levels, hot	0.485			*d*
HO production by $O(^1D)$+isobutane	2.0E−10 $molecule^{-1}cm^3s^{-1}$			*e*
nascent fraction in $X^2\Pi_{3/2}$, $v''=0$, N=1	0.1956			*f*
nascent fraction in $X^2\Pi_{1/2}$, $v''=0$, N=3	0.0737			*f*
HO absorption line width, 290K	0.1 cm^{-1}			*g*
HO nascent line width, $O(^1D)+H_2O$	0.3 cm^{-1}			*h*
HO peak absorption coefficients (A,1 ← X,0)				
$Q_1$1	1.43E−15 cm^2			*g*
Q_{21}1	1.01E−15 cm^2			*g*
$R_2$3	9.77E−16 cm^2			*g*
	Q1	V	Q0	
HO A relaxation				
by dry air	6.3E−11	1.96E−10	4.E−11 $molecule^{-1}cm^3s^{-1}$	*i*
by H_2O	6.8E−10	3.3E−10	7.9E−10	*j*
by isobutane			1.03E−9	*k*
Rotational relaxation				
A, $v'=0$, low N	2.69E−10 $molecule^{-1}cm^3s^{-1}$			*i*
X, $v''=0$, low N	2.69E−10			*l*
X, $v''=0$, high N	2.2E−10			*h*
HO A spontaneous emission (A_{11}, A_{00})	1.43E6 s^{-1}			*m*

[a] *Molina and Molina* [1986]; 3.2E−18 = 3.2×10^{-18}.
[b] *DeMore et al.* [1987].
[c] *Michaud et al.* [1974].
[d] *Cleveland* [1988].
[e] *Paraskevopoulos and Cvetanović* [1969].
[f] Calculated from rotational partition function.
[g] *McGee and McIlrath* [1984].
[h] *Gericke and Comes* [1982].
[i] Q1, V, R: *Burris et al.* [1988]; Q0: *German* [1976].
[j] Q1: *Copeland et al.* [1988]; Q0: *Copeland et al.* [1985]; V: *Chan et al.* [1983].
[k] This work.
[l] Assumed for modeling purposes.
[m] *German* [1975].

negative offsets appropriate to the ambient HO data are on the order of 0 to 2×10^6 cm^{-3}. The lines through each of the four data sets in Figure 6 are drawn from the chemical-physics theoretical model developed below, using the kinetic coefficients listed in Table 4. This model quantitatively separates all four effects, whose magnitudes are then given in Table 5.

Although the isobutane modulating reagent does introduce a small negative offset (Figure 6), it is smaller than the net interference that occurs in spectral modulation (Figure 7), and this remains true at any laser flux or tropospheric composition. Under conditions of very low laser flux the latter distinction becomes weak. However, in the presence of varying background sources or varying laser energy a further advantage of chemical modulation is that one laser and one detection cell with two sampling channels yield simultaneous measurements of both HO and the background. In comparison, to achieve similarly continuous measurements with spectral modulation, *Rodgers et al.* [1985] have used two dye lasers closely spaced in time, one laser on the HO absorption line and the other off-line, and vice versa.

Moreover, one may use chemical modulation for ambient HO measurement, and at suitable intervals use spectral modulation to detect the resonant background. One such approach, suggested by *Smith and Crosley* [1990], employs excitation transitions arising from hot groundstate HO rotational levels populated by reaction (R3). An alternative approach (also at suitable intervals during chemical modulation) is to use conventional spectral modulation around the excitation line employed in ambient HO detection; differences between the spectral and chemical net signals (the latter

TABLE 5. FAGE2 Interference Model Results, at 50 ppb O_3 and 10 Torr H_2O

Effect	Single Pass	Multipass
1. Gross resonant background	10.3	77.6
2. $O(^1D)$ competition	0.0007	0.005
3. Quenching of spurious HO^*	0.062	0.47
4. $O(^1D)$ + i-BuH → HO	−0.34	−2.6
5. Net (2 + 3 + 4)	−0.28	−2.1

Results in units of equivalent ambient [HO] = 1×10^6cm^3. See text for explanation of effects.

corrected for modulation efficiency) represent the unwanted resonant background, which is a potential source of net interferences. Of these two methods the former recognizes only rotationally hot interference sources, whereas the latter recognizes all interference sources.

A still better way to eliminate photochemical interferences is by reaction time modulation. In this method an injection loop is added to each flow tube several centimeters before the excitation zone, and the reaction time is modulated by alternating the position of reagent injection within each flow tube. Thus the reagent concentration in the laser excitation zone can be kept constant during the modulation cycle. Then interactions of the reagent with laser photolysis products (such as $O(^1D)$ and HO) lead to equal contributions to B_1 and B_2 in equation (2). These effects, if present, would contribute to the total background, but their subtraction would yield no net interference.

THEORY

The instrumental detection efficiency is not the same for HO created by the laser via the O_3+H_2O or O_3+isobutane photochemical paths as it is for ambient HO, for several reasons. First, expansion of the ambient HO and photochemical reactants to low pressure decreases the first-order rates of the kinetic steps to photochemical HO [*Hard et al.*, 1980, 1984], compared with those encountered with detection at atmospheric pressure. Second, photochemical HO grows nonlinearly during the laser pulse [*Hanabusa et al.*, 1977], exposing it to the excitation for a shorter time (on the average) than is the case with ambient HO. Third, the O_3+H_2O path produces a highly nonthermal rotational distribution [*Gericke and Comes*, 1980; *Rodgers et al.*, 1981; *Butler et al.*, 1981; *Gericke et al.*, 1981; *Comes et al.*, 1981; *Gericke and Comes*, 1982; *Cleveland*, 1988] and a hot translational distribution [*Gericke et al.*, 1981, *Gericke and Comes*, 1982]. Fourth, the transient laser flux leads to different degrees of radiative saturation of the ambient and spurious HO populations probed by the laser [*Smith and Crosley*, 1990]. Fifth, the reagent used for chemical modulation of ambient HO may alter the fluorescence efficiency of the HO-resonant part of the background.

Reagent addition adds processes to those already controlling the behavior of the emitting state, leading to the potential interferences 2 and 3 described above. Without gating, the HO fluorescence efficiency at 309 nm after pulsed excitation at 282 nm is

$$E_F = \frac{k_V[\mathrm{M}]+k_{Vi}[i\text{-BuH}]}{A_{11}+(k_{Q1}+k_V)[\mathrm{M}]+(k_{Q1i}+k_{Vi})[i\text{-BuH}]} \times \frac{A_{00}}{A_{00}+k_{Q0}[\mathrm{M}]+k_{Q0i}[i\text{-BuH}]} \quad (5)$$

in which the first fraction is the efficiency with which the initially excited $v'=1$ state relaxes vibrationally to the emitting state $v'=0$, relative to the total loss rate of $v'=1$ by radiative emission (A), quenching (k_{Q1}[M]), and vibrational relaxation (k_V[M]). The second fraction is the efficiency of $v'=0$ radiative emission, similarly affected by the quenching loss k_{Q0}[M]. Although the terms containing k_{Q1i}, k_{Vi}, and k_{Q0i} (i = isobutane) can change the fluorescence efficiency, experimental values are available only for k_{Q0i}. The latter's contribution to the change in efficiency increases when a delayed gate is applied to the HO fluorescence waveform, since an increase in quenching shortens the waveform's duration. Gating is used because the predominant noise in the detection of ambient HO is the fluctuation of the nonresonant portion of the background (i.e., not laser-produced HO), which decays more rapidly than the HO fluorescence.

In the presence of a mildly saturating transient radiative flux and nonequilibrium nascent energy distributions, the kinetic system is most easily described by implicit integration of the differential equations for spurious HO production, excitation, relaxation, and emission [*Smith and Crosley*, 1990]. Our model is described in the appendix, and the values of the parameters used in the computations are listed in Tables 1 and 4. The resulting gross resonant backgrounds and net interferences are presented in units of the signal for an ambient HO concentration of 1 x 10^6 molecules cm^{-3}, whose excitation and emission are calculated by the same kinetic model. The model-calculated HO A $(v'=0)$ production and loss were integrated over the gate period used in the ambient measurements and interference experiments. Numerical results for the resonant background and three identified contributions to the net interference are given in Table 5.

The radiative saturation parameter S, defined as the population ratio between the upper and lower levels of an absorbing transition, is represented here by the time-dependent average of such ratios of the three probed transitions, weighted by the respective populations of their lower levels in the absence of saturation. Figure 10 shows the calculated time dependence of S_a (ambient HO), S_w (HO from reaction (R3)), and S_i (HO from reaction (R4a)) during the laser pulse. Relative to S_a, the denominators of S_w and S_i are raised by the influx of new HO into the lower levels during the pulse, and the numerator is lowered by exposure of this HO to stimulating radiation for a shorter average period. S_w is also affected by higher values of the absorption coefficient σ_{eff} (appendix). At the end of the first laser pass through the sample, S_a, S_w, and S_i are equal to 0.59, 0.28, and 0.17, respectively. It is clear that none of these terms has reached the saturation limit of unity. The ambient HO absorption is more highly saturated than the photochemical HO terms; if saturation were removed, the ambient HO

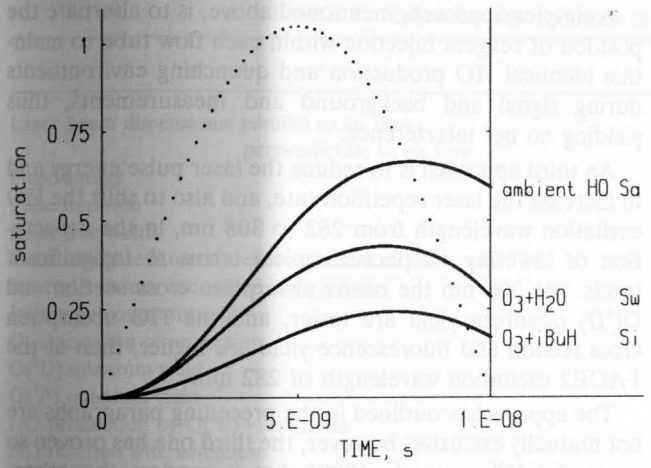

Fig. 10. Saturation (as defined in text) versus time, for the signal due to ambient HO and for the two photochemical HO sources (solid lines). Dotted line: YAG/dye excitation waveform used in model.

response would be 2.5 times greater, but the normalized net interference and resonant background would decrease by only 35% and 32%, respectively. (The latter case was simulated by using artificially high rotational relaxation rates for $A\ (v'=1)$ and for the cold portion of groundstate HO.)

Table 5 indicates an interference level for the excitation conditions in single-pass mode which is below the instrumental 2σ detection limit for 1-hour averaging time. However, interaction of multiple laser passes increases this interference to a level which is significant relative to ambient HO concentrations. The spatial overlap among the laser passes in the White cell is too complex to be modeled in full detail; we calculated multipass ambient HO signals by multiplying the single-pass model prediction by the measured multipass/single-pass ratio of the ambient HO response (this value was measured to be 8.0). Similarly, we calculated the multipass gross resonant background by multiplying the singlepass prediction by the measured multipass/singlepass ratio of resonant backgrounds (we measured this to be 7.5). Also, in order to evaluate the processes that account for the observed multipass increases we modeled the results of a second laser pulse with a typical time delay of 15 ns and varying spatial overlaps with the first pulse. The modeling procedure, which takes into account the measured alternation in successive beam diameters (0.6 and 0.4 cm) in the White cell, is described at the end of the appendix. The value of spatial overlap which brings the model-predicted and experimentally observed multipass/single-pass ratios of gross photolytic backgrounds into agreement is 30%.

In agreement with the results of *Smith and Crosley* [1990] we find that the largest contributor to the multipass increase is the persistence of $O(^1D)$ that was generated in the first pulse, leading to continued HO production and accumulation before and during the second pulse. A smaller contribution to the increase is rotational relaxation of hot HO.

With the calculated photon collection/detection efficiency of 1/36 (solid angle at f:1.5 relative to sphere) times 0.5±0.2 (off-axis losses) (quoted uncertainties are 1σ estimates) times 0.28±0.05 (mean filter transmission) times 0.5±0.1 (overlap of filter with 0,0 emission) times 0.6±0.1 (window and lens transmission) times 0.22±0.02 (photomultiplier quantum efficiency) = 2.6×10^{-4} (±50%), as well as the observed multipass/single-pass ratio, the model predicts an HO response of 0.057 photons per laser pulse per 1×10^6 HO cm^{-3}, in reasonable agreement with the response of 0.04 (same units) obtained by independent calibration [*Hard et al.*, 1986]. Comparison of the latter predicted and observed HO responses implies a chemical HO loss of 30% in sampling. However, given the large uncertainty in the predicted response, we have instead used a chemical loss of approximately 2% which brings interference observations and model into agreement.

The predicted multipass net interference versus $[H_2O]$, using our measured value for k_{Q0i}, is compared with the experimental data in Figure 6. As elsewhere in this work, the model's values are normalized to the signal from ambient HO, and the ambient HO loss in the nozzle and tube is used as an adjustable parameter (Table 1) to fit the interference data; its actual value may differ from the "best fit" value of 2%. The fit of the model to the data is not perfect, particularly at the lowest isobutane concentration. However, the negative intercept and positive slope versus $[H_2O]$ of the data are reproduced by the model. The intercept is identified with the O_3+isobutane interference (effect 4 above), and the slope is identified primarily with quenching of the increasing O_3+H_2O background by the constant isobutane (effect 3). As noted above, the value of k_{Q0i} reported by *Wysong et al.* [1990] generates slopes which are also consistent with the interference data.

The predicted single-pass net interference, or offset, at 1% H_2O is plotted as a function of average laser power in Figure 11. The deviations of this result from linearity are due to the differences in saturation behavior (Figure 10) among the interference terms and the ambient HO signal. For convenience, the multipass prediction is shown as a single point at the single-pass flux value; actually, partial spatial overlap of successive beams tends to raise, and mirror reflection losses tend to lower, the effective value of the multipass flux.

The predicted time to reach snr = 2 (using twice the uncertainty $(e_M)_{est.2}$ defined in equation (4*b*)) is plotted as a function of average laser power in Figure 12. In these

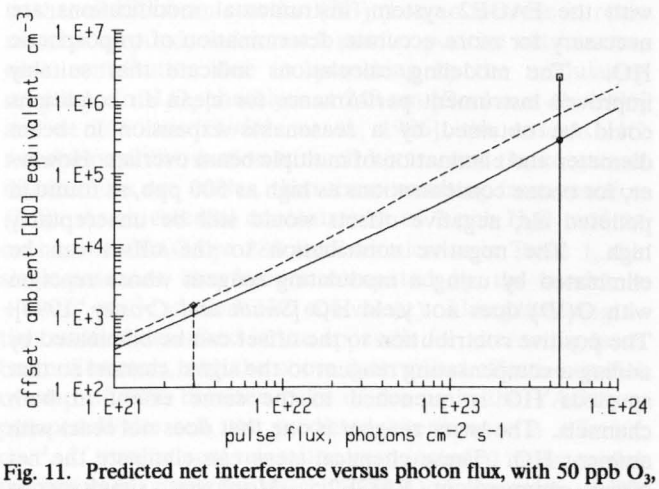

Fig. 11. Predicted net interference versus photon flux, with 50 ppb O_3, 10 torr H_2O. Solid lines: YAG/dye 282-nm single-pass excitation (sign of interference is negative); dashed lines: Cu/dye 308-nm single-pass excitation, with back-diffusion (sign of interference is positive). Point symbols correspond to present excitation conditions: open circles: YAG/dye single-pass; open squares: YAG/dye multipass; open diamonds: Cu/dye single-pass, with back-diffusion. Sinewave (positive lobe) excitation; flux units refer to equivalent square wave (same FWHM and same area).

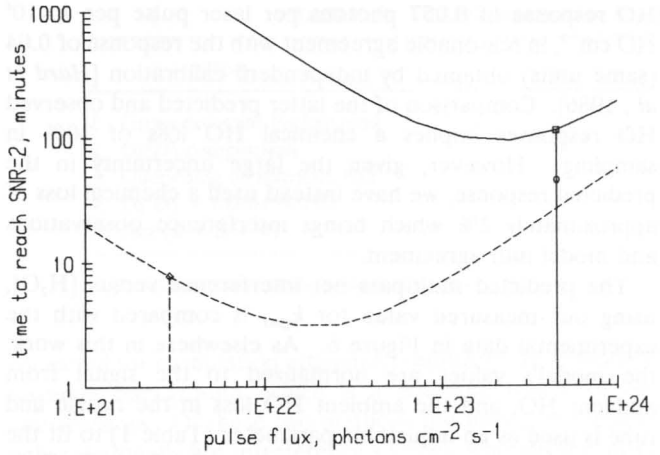

Fig. 12. Predicted averaging time required to reach snr = 2 at ambient [HO] = 1×10^6 molecules cm^{-3}, taking into account both predicted resonant background and measured nonresonant background. Symbols and flux units same as in Figure 11.

predictions the total background $(B_1 + B_2)$ includes both HO-resonant and nonresonant terms. The value used here for the nonresonant background is the largest observed at any time during the ambient HO determinations in Figure 1 and may contain contributions from fluorescence of aerosols, of gases other than HO, and of the walls of the cell. This nonresonant background is larger than that observed earlier [*Hard et al.*, 1986]. Starting at the left side of Figure 12, where the laser flux is small, the mean net signal is proportional to flux, and its estimated uncertainty is proportional to the square root of the flux; so the required averaging time to reach snr = 2 decreases with increasing flux in this region. With further growth in flux the required averaging time increases, due to partial saturation of the excitation transition and to the nonlinear increase in the resonant background due to laser-produced HO in both channels.

Given the small but significant negative offsets obtained with the FAGE2 system, instrumental modifications are necessary for more accurate determination of tropospheric HO. The modeling calculations indicate that suitably improved instrument performance for clean air conditions could be obtained by a reasonable expansion in beam diameter and elimination of multiple beam overlap. However, for ozone concentrations as high as 500 ppb, as found in polluted air, negative offsets would still be unacceptably high. The negative contribution to the offset can be eliminated by using a modulating reagent whose reaction with $O(^1D)$ does not yield HO [*Smith and Crosley*, 1990]. The positive contribution to the offset can be eliminated by adding a compensating reagent to the signal channel so that spurious HO is quenched to the same extent in both channels. The latter reagent is one that does not react with ambient HO. These chemical steps can eliminate the net offset observed in FAGE2. Moreover, simultaneous reduction of both the laser flux and the laser line width by a factor of 3 (to match the HO absorption line width) could improve the snr of the FAGE2 system by a factor of 1.6, and the required averaging time by a factor of more than 2. However, the price paid for decreasing the laser line width is reduced wavelength stability of the instrument.

A simpler approach, mentioned above, is to alternate the position of reagent injection within each flow tube to maintain identical HO production and quenching environments during signal and background and measurements, thus yielding no net interference.

An third approach is to reduce the laser pulse energy and to increase the laser repetition rate, and also to shift the HO excitation wavelength from 282 to 308 nm, in the expectation of lowering all photochemical terms to insignificant levels. At 308 nm the ozone absorption cross section and $O(^1D)$ quantum yield are lower, and the HO absorption cross section and fluorescence yield are higher, than at the FAGE2 excitation wavelength of 282 nm.

The approaches outlined in the preceding paragraphs are not mutually exclusive; however, the third one has proven so successful [*Chan et al.*, 1990] that it renders the others unnecessary.

The dashed lines in Figures 11 and 12 are offset and snr computations for 308 nm excitation, appropriate to the FAGE3 instrument [*Chan et al.*, 1990]. This instrument uses a Cu vapor laser to pump the tunable dye laser, whose output is frequency doubled as above. The Cu/dye laser's average power is about one third of that of the YAG/dye system described here and its pulse repetition rate, 5.6 kHz, is a factor of 187 higher; thus its lower pulse energy and shifted excitation wavelength lead to much lower photochemical interference. Table 6 gives values for those Cu/dye parameters whose values differ from those of the YAG/dye system in Tables 1 and 4. As pointed out by *Smith and Crosley* [1990], back-diffusion of spurious HO from one laser-excited volume to the next, accompanied by further HO production during the elapsed time interval, can lead to substantial increases in photochemical interference. The diffusive overlap (i.e., the fraction of the initially irradiated air that spreads by diffusion into the next excitation volume during the interval between laser pulses) can be estimated by a one-dimensional diffusion model using the 1 mm thickness of the laser excitation volume normal to the sample flow, the estimated plug-flow velocity of 1400 cm s^{-1}, the 5.6-kHz laser repetition rate, and Smith and Crosley's estimate of $D = 60$ cm^2/s for the diffusion coefficient of HO. (Since the excitation volume is only 3 mm wide rather than an infinite sheet, and since the air velocity in the excitation/detection region appears to exceed the plug-flow velocity, the estimate of the diffusive overlap is likely to be conservatively large.) The calculation may be performed either iteratively in time and space (as was done by Smith and Crosley) or more efficiently via superposition of Gaussians. In the latter method, at time t equal to the laser repetition period, the final population in the volume element centered at point x_j is $n_j = \Sigma_i(4Dt/\pi)n_i\exp[-(x_i-x_j)^2/(4Dt)]$, which is the sum of the contributions of the initial populations n_i at each x_i of the initial distribution. The x_j of interest are obtained by translation of the initially populated x_i by vt (v=flow velocity), and the corresponding n_j are summed and normalized to the sum of n_i to yield the diffusive overlap. Both the iterative and the direct methods yield a value of 0.068 for the diffusive overlap under the above conditions. The diffusive overlap of laser pulses separated in time by $2t$ is 1.6×10^{-5}, yielding negligible added interference in this chemical system from nonadjacent pulses.

TABLE 6. Quantities Used in Ozone Interference Model, Cu/Dye 308-nm Excitation

	Value	Notes
Laser beam dimensions: parallel to air flow	0.1 cm	*a*
perpendicular to air flow	0.3 cm	*a*
Pulse energy	1.0 μJ	*a*
Pulse duration	16.67-ns FWHM, 25-ns base width	*a*
Laser line width	0.3 cm^{-1}	*a*
Detection gate interval, relative to start of laser pulse	60 to 360 ns	*a*
Interval between successive laser pulses	179 μs	*a*
Isobutane concentration	430 ppm	*a*
O_3 absorption cross section	1.36E−19 cm^2	*b*
$O(^1D)$ quantum yield	0.74	*c*
$O(^3P)$ quantum yield	0.26	*c*
HO production by $O(^3P)$+isobutane	1.0E-13 $molecule^{-1}cm^3s^{-1}$	*d*
HO reaction with isobutane	2.36E-12	*e*
HO peak absorption cross sections (A,v'=0 ← X,v"=0)		
$Q_1 1$	5.60E−15 cm^2	*f*
$Q_{21} 1$	3.97E−15 cm^2	*f*

Quantities are listed whose values differ from or are not found in Tables 1 and 2.
[a] Measured.
[b] *Molina and Molina* [1986].
[c] *DeMore et al.* [1987].
[d] *Washida and Bayes* [1980].
[e] *Darnall et al.* [1978].
[f] *McGee and McIlrath* [1984].

During the first 3 μs after one laser pulse the disappearance of $O(^1D)$ and the thermalization of rotationally hot HO both reach completion. Throughout the remaining 176 μs before the next pulse there is persistent groundstate HO production by the reaction of groundstate O atoms ($O(^3P)$) with isobutane and by the relaxation of vibrationally hot HO. The chemical-kinetic model calculations start at the beginning of one laser pulse, with no prior contribution of spurious HO. All transient O and HO species are reduced by the previously calculated diffusive overlap before ozone photolysis resumes in the second laser pulse. Execution stops at the end of the second pulse's signal integration interval. The integrated signals from the second pulse alone, without and with isobutane present, are added to obtain the gross resonant background or subtracted to yield the net interference, and these results are normalized to those of ambient HO. The calculated gross resonant background is 1.9×10^5 cm^{-3} (ambient HO equivalent), a factor of 14 greater than in the absence of diffusion; the net interference changes from -2×10^2 cm^{-3} without diffusion to $+1.4\times10^3$ cm^{-3} with diffusion. (The change in sign of the net interference indicates that more groundstate HO is produced by the thermalization of rotationally and vibrationally hot HO than by the reaction of $O(^3P)$ with isobutane.)

Thus the predicted net interference in FAGE3 at 50 ppb O_3 and 10 torr H_2O is below the experimental detection limit of the instrument [*Chan et al.*, 1990]. (The predictions of net interferences in Figure 5 of the latter paper were calculated for the absence of diffusion; this and other revisions require multiplication of the spectral-modulation curve in that figure by a factor of 20 and the chemical-modulation curve by a factor of −3.) The single-pass design of the FAGE3 instrument has permitted reduction of beam mask sizes from those used in FAGE2, greatly lowering the measured nonresonant background due to cell fluorescence. Moreover, the detected fluorescence of ambient air components (other than HO) appears to be smaller when the excitation and detection wavelengths are closer (i.e., 308 and 309 nm versus 282 and 309 nm). Both of the latter effects are reflected in the reduced averaging time found with FAGE3 [*Chan et al.*, 1990] and illustrated by the dashed curve in Figure 12.

The model is also used to predict interference associated with YAG/dye photolysis of ambient H_2O_2 to produce HO, using the values in Table 7. In this case, as well as for other ambient HO-containing species that are photolyzed by the UV laser, the model predicts behavior qualitatively similar to that of HO from reaction (R3) (i.e., an increase in resonant background, and a much smaller positive net interference contribution due to quenching by the modulating reagent). In H_2O_2 photolysis at 248 nm [*Docker et al.*, 1986] and at 266 nm [*Gericke et al.*, 1986], the nascent HO translational distribution is much hotter, and the rotational distributions are cooler, than those resulting from reaction (R3). At an external concentration of 3 ppb H_2O_2 and no ozone, with YAG/dye 282 nm excitation as in Table 1, the single-pass net interference computed by the model is $+4\times10^4$ cm^{-3} (ambient HO equivalent). Using the integration method described in the appendix for alternating laser beam diameters, with the above determined effective spatial overlap of 30% between pairs of beams in the YAG/dye-pumped White cell, the predicted interference is $+7\times10^4$ cm^{-3}. If translational relaxation were included in the model for this case, given the nascent HO Doppler width of 0.8 cm^{-1}, the maximum possible increase in σ_{eff} in equation (A1) would be a factor of 2. An upper limit to the YAG/-dye multipass H_2O_2 interference is thus $+7\times10^4 \times 2 = +1.4\times10^5$ cm^{-3}. With Cu/dye 308 nm excitation as in Table 6, including the effects of back-diffusion, the computed interference due to 3 ppb H_2O_2 is $+1\times10^2$ cm^{-3}.

TABLE 7. Quantities Used in Model of H_2O_2 Interference in FAGE2

	Value	Notes
H_2O_2	3.0 ppb	*a*
H_2O_2 absorption coefficient, 282 nm	1.8E−20 cm^2	*b*
Nascent HO line width	0.8 cm^{-1}	*c*
Nascent fraction in $X^2\Pi_{3/2}$, $v''=0$, N=1	0.066	*c*
Nascent fraction in $X^2\Pi_{1/2}$, $v''=0$, N=3	0.06	*c*
Nascent fraction in other "cold" $v''=0$ levels	0.237	*a*
Nascent fraction in "hot" $v''=0$ levels	0.7	*a*
Rotational relaxation coefficient for "hot" HO	2.69E−10 $molecule^{-1}cm^3s^{-1}$	*a*

[a] Assumed for modeling purposes.
[b] *DeMore et al.* [1987].
[c] *Gericke et al.* [1986].

Sensitivity to Input Variables

The model for the YAG/dye system (described in the appendix) has been tested for the sensitivity of its predictions to variations in the values of quantities describing the instrumental conditions as well as in values of the kinetic coefficients. The model's greatest sensitivity is to the UV laser beam diameter: a 10% increase produces a 32% decrease in the net interference. The other experimental quantities yielding a major sensitivity are the wave shape chosen to represent the laser pulse, and the pulse energy. Figure 2 superimposes the measured laser waveform on a square wave, the half sine wave used here, and the truncated Gaussian used by *Smith and Crosley* [1990], all with the same area and FWHM. A change from half sine wave to truncated Gaussian raises the net interference by 18%. A 10% increase in the laser pulse energy gives a 13% rise in net interference. The predicted net interference is linear in O_3 and isobutane. Laser pulse width, detection pressure, and laser line width, when their individual values are separately increased by 10%, respond with +8%, +5%, and −3% changes in predicted net interference, respectively.

The negative sensitivity to the laser line width may seem counterintuitive, but it is the result of two effects that are qualitatively understandable. First, in using equation (A1) (appendix) to calculate the changed absorption cross-sections, the σ_{eff} of both ambient HO and the interference from reaction (4*a*) decrease to a greater extent than the σ_{eff} of the HO from reaction (R3). This increases the normalized resonant background as well as the (positive) quenching contribution to the net interference. The second effect is due to the differing degrees of saturation shown in the solid curves in Figure 10. Relative to the ambient HO signal, the O_3+isobutane interference is less saturated and therefore decreases more rapidly upon the decrease in their common σ_{eff}, yielding a reduction in this negative interference.

Among the model's kinetic parameters, proportional changes in the net interference are produced by the coefficients for reactions (R1) and (R4*a*). All other kinetic coefficients of the model, in response to a 10% change in their values, lead to changes of less than 3% in the predicted net interference. Therefore the greatest sensitivities of the model are to the instrumental variables, especially the laser beam diameter.

Error propagation, using model sensitivities that arise from the experimental uncertainties in Table 1, gives a 35% uncertainty in the predicted net interference due to instrumental parameters. For a set of parameters similar to those in Table 2, *Smith and Crosley* [1990] have estimated a model uncertainty of 50% due to uncertainties in the kinetic parameters. Combining their 50% result with our 35% model uncertainty due to instrumental variables, we obtain 61% for the overall uncertainty in our predicted net interference.

Comparison With Other Models

Of the interference models listed in the introduction, only *Ortgies et al.* [1981] and *Smith and Crosley* [1990] address the effects of saturation on interference. The treatment by *Ortgies et al.* [1981] ignores rotational hole filling in the ground and excited states (a relatively small effect) but was not intended to address the effects of chemical modulation of HO.

Like the present model, Smith and Crosley's is intended to describe FAGE2 and to explore possible improvements. They obtain nascent populations of the laser-probed HO levels (reaction (R4*a*)) from the approximate fitted temperatures of the hot and cold parts of the rotational distribution, while we obtain the populations for the probed levels directly from Figures 4.5 and 4.6 of *Cleveland* [1988].

The most significant difference between the Smith and Crosley model and ours concerns the input data for the FAGE2 instrument. Smith and Crosley use values for the reaction tube length and the laser line width taken from our description of the first-generation FAGE1 instrument [*Hard et al.*, 1984], which used a shorter flow tube (accounting for the lower chemical modulation efficiency calculated by Smith and Crosley) as well as a different laser system. Actual values for the FAGE2 instrument, which was incompletely described by *Hard et al.* [1986] and was used to obtain the YAG/dye interference data reported here, are given in Table 1. More justifiably, for the laser beam diameter Smith and Crosley use the value of 0.4 cm we reported in the work by *Hard et al.* [1989], while we use the larger value of 0.6 cm, the diameter of the first laser pass, in order to make use of our measured multipass/single-pass ratios. We feel that the latter approach is more meaningful, since values of the actual beam spatial overlap of successive laser passes are impossible to obtain experimentally for use in the model. The difference in beam diameters leads to severalfold higher net interference for the single pass case in Smith and Crosley's model than in ours. For the multipass case these differences are partly canceled by Smith and Crosley's lower effective spatial overlap of 10% between adjacent beams in

the White cell, compared with our experimentally constrained 30% overlap. Thus for 50 ppb ozone and 10 torr H_2O, Smith and Crosley's calculated multipass net interference is equivalent to -4×10^6 cm^{-3} ambient HO, twice that shown in Table 5.

Similarly, for the FAGE3 Cu/dye system [*Chan et al.*, 1990], Smith and Crosley use input parameters based on earlier stages of development of that instrument, before the homebuilt dye laser had been optimized for HO detection or had been used to explore the merits of 308-nm excitation. Thus Smith and Crosley assumed HO excitation at 282 nm, where O_3 and other photolytic parents absorb more strongly than at 308 nm, and used a laser pulse energy 15 times as great as we eventually employed in FAGE3.

We have attempted to replicate the calculations of *Smith and Crosley* [1990] for both the FAGE2 and FAGE3 systems, using their choice of instrumental conditions, their chemical mechanism, and a Gear-based chemical kinetics program. To obtain agreement with their results for FAGE2, we found it necessary to introduce two modifications to their chemical mechanism. First, the values given for the absorption cross sections for hot nascent HO produced by reaction (R3) and for ambient HO in Table 1 of *Smith and Crosley* [1990] are inconsistent with the description given in their text; thus we multiplied their quoted "hot" HO absorption cross sections by 2.48, obtained from their values of the linewidths of the laser, ambient HO, and "hot" HO via equation (A1) of the appendix. Second, since radiative excitation can be faster than rotational relaxation in this system, we distinguished the A $(v=1)$ rotational states of translationally "hot" HO from those of thermalized HO, and allowed the former to relax to the latter with rate coefficients derived from that of rotational relaxation in the A state.

With the latter modifications the results of the replication agreed closely with those of Smith and Crosley in the YAG/dye 282-nm FAGE2 case, yielding a net interference of -8×10^6 cm^{-3} (ambient HO equivalent) for their input concentrations of 100 ppb O_3 and 10 torr H_2O. However, the replication disagreed strongly with their results in the Cu/dye 282-nm FAGE3 case. Without back-diffusion they reported a net interference of -2×10^5 cm^{-3} where the replication yielded a higher value, -3.4×10^5 cm^{-3}. With back-diffusion included they reported a net interference of $+8\times10^6$ cm^{-3}, whereas the replication yielded $+1.4\times10^6$ cm^{-3} for the net interference, nearly a factor of 6 smaller than their result. Given the close agreement for the FAGE2 case and the discrepancy of less than a factor of 2 for the FAGE3 diffusion-free case, we suggest that the disagreement in the FAGE3 back-diffusion case arises either in the diffusive overlap value or the way in which it is folded into the chemical-kinetic model calculations. Smith and Crosley do not provide a value for the diffusive overlap; we obtained an overlap of 0.049 using their quoted 0.2-cm beam thickness, 5000-Hz laser repetition rate, and 1850 cm s^{-1} flow speed.

Remember that the replication of Smith and Crosley's model is based on input conditions far from those actually used in the experiments of *Chan et al.* [1990]: the net interference for real conditions in the Cu/dye 308-nm case is yet another factor of 1000 smaller. The largest contributors to this improvement are the 15-fold lower laser energy used and the 28-fold lower cross section for $O(^1D)$ production in ozone photolysis at the 308-nm excitation wavelength compared with that at 282 nm.

On the basis of the large interference levels yielded by their model of the Cu/dye system, Smith and Crosley recommended the use of a fully deuterated modulating reagent in the background channel and a second reagent in the signal channel to balance the added quenching in the background channel, or else a severalfold decrease in repetition rate of the Cu laser to reduce the effects of back-diffusion. These corrective measures might be appropriate if the actual HO excitation conditions were those they cited; however, the actual conditions used by *Chan et al.* [1990], being a thousandfold less severe, do not require the use of these reagents to achieve negligible interference. Moreover, in both FAGE2 and FAGE3 the largest dimension of the detection region (the intersection of the detector's field of view with the laser-excited volume) is only 40% of the flow tube diameter, to avoid detection of scattering by the walls nearest the laser beam. Thus diffusion in the slower-moving air near the flow tube walls, cited as a problem by Smith and Crosley, does not contribute to the detected interference.

We agree with *Smith and Crosley* [1990] that these models should not be used to apply corrections to ambient HO data, even if ozone, H_2O, and H_2O_2 have been measured simultaneously. The uncertainties in the models' rate coefficients and instrumental input data are too large to justify such corrections. Rather, the model calculations should be used to ensure that experimental measurements of the ozone interference (which are simple to carry out) are in agreement with photochemical theory and therefore that evolving HO instrumentation is demonstrably free from known photochemical interferences.

INTERFERENCES IN PREVIOUS WORK

As described above, in the YAG/dye system with chemical modulation the experimentally measured and theoretically calculated offsets are always negative and are in reasonable agreement with the ambient measurements reported here (Figure 1). Previous ambient HO data [*Hard et al.*, 1986] were obtained with the same FAGE2 YAG/dye instrument described in the experimental section of the present paper. The data we reported for June 17-19, 1985 show a diurnal variation, with small or zero signals at night and positive signals in the day. Those data were displayed as a 1-hour moving block average, with moving error bars equal to ±2 times the photon-counting uncertainty defined in equation (4*b*). In this case, $S + B_1$ and B_2 were the total photon counts in the respective 1-hour sums. Although simultaneous ozone measurement was attempted, the $O_3+C_2H_2$ chemiluminescence monitor suffered from extreme zero drift which could not be repaired during the experiment. The present experimental and theoretical results indicate that whenever ozone was present, true ambient HO concentrations in the June 1985 ambient data were somewhat larger than reported, due to negative offsets whose order of magnitude may be inferred from the nighttime data in Figure 1.

An earlier measurement of ozone interference in FAGE1 [*Hard et al.*, 1984], employed a different YAG/dye laser, sampling cell, and detection system. The interference measurement was obtained with spectral modulation, unlike the ambient data reported in that paper. At an estimated

TABLE 8. Quantities Used in Ozone Interference Model of FAGE1

	Value	Notes
Detection total pressure	4 torr	*a*
O_3	4 ppm	*b*
H_2O	10 torr	*b*
Beam diameter, single laser pass	0.2 cm	*a*
Pulse energy	0.1 mJ	*a*
Pulse duration	6.67-ns FWHM, 10-ns base width	*a*
Laser line width	0.5 cm^{-1}	*a*
Detection gate, relative to start of laser pulse		
at 4 torr	110 to 270 ns	*a*
at 150 torr	0 to 270 ns	*a*

[a] Measured in the work by *Hard et al.* [1984].
[b] Assumed for modeling purposes.

ozone concentration of 4 ppm and 45% relative humidity and 4 torr, we reported no detectable interference "at the 10^6 level," and at 150 torr a detectable interference equivalent to 8×10^7 cm^{-3} HO. With the relevant quantities listed in Table 8, the present model predicts 5.4×10^8 cm^{-3} at 4 torr and 1.9×10^{10} cm^{-3} at 150 torr. These values are in qualitative agreement with *Shirinzadeh et al.* [1987*a*], being larger by factors of 1.2 and 2.4 respectively, than those used by Shirinzadeh et al. to criticize this experiment; the differences arise both from improved rate coefficients and the inclusion of saturation in the present model. However, with the calculated photon collection efficiency appropriate to the older system the model agrees well with the HO response obtained by calibration. Therefore we believe that the very large discrepancies in the interference measurements reported in 1984 were due to an indirect measurement of the ozone concentration before dilution by room air, and delivery of ozone perpendicular to, and at a distance from, the axis of the sampling nozzle, resulting in much greater dilution than we estimated. That procedure contrasts with the present one, in which ozone is delivered along the nozzle axis after dilution with a flow of pure air that is sufficient to exceed the nozzle flow requirement, and in which the ozone concentration is continuously measured just before entering the nozzle.

Although our 1984 measurement of the photolytic interference which would result from spectral modulation was obviously in egregious error, there are no direct consequences for ambient data or calibrations reported by us in either 1984 or 1986, since chemical modulation was used in all our reported measurements. Nevertheless, this erroneous measurement gave us false confidence that net photochemical interference would be entirely negligible in the ambient HO data in the 1984 and 1986 papers.

The results of the present interference experiments and calculations indicate that significant HO-resonant background may have been present during the ambient HO measurements we reported in the work by *Hard et al.* [1986], as was first pointed out by *Shirinzadeh et al.* [1987*a*]. However, the net interference calculations of the latter authors were based on an incorrect interpretation of the $O(^1D)$ competition mechanism at low pressures, resulting in an overestimate of this contribution by a factor of 1000 as well as a disagreement in sign with the observed interference, as noted by *Hard et al.* [1989]. The contribution of the latter mechanism to the net interference is negligible. Nonetheless, since other mechanisms not considered by Shirinzadeh et al. can produce significant interferences of either positive or negative sign during chemical modulation, the latter authors' concern was justified.

Our 1986-reported data also have been criticized by *Smith and Crosley* [1990], based upon their chemical-physics model of the excitation process discussed above. We believe that their conclusion that the 1986-reported data are invalid are not supported by the stated uncertainties in their calculations, for which they estimate an uncertainty of ±50% due to rate constant uncertainties, and yet another factor of 2 or 3 due to uncertainties in the experimental parameters such as beam diameter, laser power, etc. As with the present ambient HO data, the observed positive daytime signals in the 1986-reported data contrast with the negative net interference measured experimentally here and predicted by both their model and ours. However, the occurrence of negative offsets in the presence of ozone, with the absence of ozone measurements in the work by *Hard et al.* [1986], do have a compromising effect on the HO data in that paper. Nevertheless, we believe that the major stated conclusions in that paper still stand. These conclusions were that a diurnal cycle of ambient HO had been observed in June 1985 and that much lower concentrations (along with a small negative offset) were present in November 1985. The diurnal cycles and measured concentrations were stated to be in rough agreement with tropospheric models. Certainly, in the absence of ozone measurements and absolute UV data the HO data were not used to "test" any tropospheric model. The peak ambient HO concentrations we reported in the June 1985 data are comparable with the peak HO observed in the two ambient HO data sets presented in Figure 1 of this paper, for which the ozone concentrations are known, and in which we observe negative offsets in agreement with laboratory-measured and model-calculated offsets.

SUMMARY

We have obtained ambient HO measurements supported by simultaneous ozone and water vapor data. The Pacific coastal measurement site provided remote marine air during daytime of the May 1987 experiment and during both day and night during the August 1987 experiment. The observed peak daytime [HO] ranged from 2.5 to 3×10^6 mole-

cules cm^{-3} (May 5-7) and from 3 to 8×10^6 molecules cm^{-3} (August 18-20). These data are within the range of values observed by independent methods at other sites. Negative offsets were observed which were small in comparison with peak daytime ambient HO, though not negligible.

Since such negative offsets are to be avoided, we have used separate experiments to measure the interferences and resonant backgrounds as functions of ozone, water vapor, and isobutane reagent concentrations. We have measured the added quenching of the detected fluorescence due to isobutane. We have developed a model to describe photochemical backgrounds and interferences in the determination of HO by low-pressure laser-excited fluorescence with chemical modulation. Such a model is useful in the design of future instruments for LEF measurements of tropospheric HO. In view of uncertainties in instrumental input data and kinetic coefficients the model's predictions must be regarded as semiquantitative. However, the laboratory experiments are consistent with the model's predictions. In particular, the observed negative offsets are due to HO production by $O(^1D)$+isobutane, while isobutane modulation of the resonant background present in both channels from $O(^1D)+H_2O$ accounts for the decrease in this negative offset with increasing water vapor concentration. At 30 ppb O_3 and 10 torr H_2O, typical of ambient HO measurements reported here, the measured offset is less than -1.3×10^6 cm^{-3} (i.e., at the upper limit of the available laser pulse energy, 0.6 mJ). If ozone was present in our previous tropospheric HO determination by FAGE2 [*Hard et al.*, 1986], then peak [HO] was underreported, due to the latter negative interference.

The dominant cause of these interference effects for clean-air HO measurement with FAGE2 is shown by the model to be due to overlap of laser beams in the White cell. The removal of this overlap would make the net interference negligible with respect to FAGE2's detection limit in remote air. In polluted air with high ozone concentrations the larger net interferences in FAGE2 can be eliminated by alternating reagent injection between two axial positions in each low-pressure flow tube. However, the latter modulation method does not remove the resonant background, which tends to degrade the sensitivity of FAGE2 at high ozone concentrations. To provide an instrument free of significant interferences in either remote or polluted air, we have elected to change the dye-pumping laser (from YAG to Cu vapor) and the dye laser wavelength (from 282 to 308 nm). This instrument, FAGE3, has completed laboratory development, testing, and calibration [*Chan et al.*, 1990] and is now undergoing field tests.

APPENDIX: MODEL DESCRIPTION

Values of the instrumental and chemical-kinetic quantities used in the model are listed in Tables 1 and 4. *Michaud et al.* [1974] reported a rate coefficient for reaction (R4) relative to that of $O(^1D) + CO_2 \rightarrow O(^3P) + CO_2$; the recommended absolute rate coefficient of the latter reaction [*DeMore et al.*, 1987] yields the rate coefficient of (R4) in Table 4. The branching ratio between reactions (R4*a*) and (R4*b*) (0.27:0.73) is inferred from the observed stable final products of reaction (R4) [*Paraskevopoulos and Cvetanović*, 1969]. The nascent HO rotational distribution resulting from (R4*a*) is assumed to be cold, in analogy with observations of the distributions from the reactions of $O(^1D)$ with propane and with neopentane [*Luntz*, 1980], and in agreement with our own observations.

HO excitation at 282 nm is achieved via three overlapping absorbing transitions (Q_11, $Q_{21}1$, and R_23) connecting two lower and three upper levels. Values of effective absorption coefficients σ_{eff} are obtained from peak absorption coefficients σ_P [*McGee and McIlrath*, 1984] via

$$\sigma_{eff} = \sigma_P \{\min(\Delta\nu_D, \Delta\nu_L)/(\Delta\nu_D^2 + \Delta\nu_L^2)^{-1/2}\} \quad \text{(A1)}$$

The stimulated absorption coefficients are the products of the values of σ_{eff} with the respective ratios between the lower and upper rotational state degeneracies. The Doppler width of HO from reaction (R3) (0.3 cm^{-1}) is roughly equal to that of the laser, leading to a higher value of σ_{eff} than in the cases of ambient HO and of HO from reaction (R4*a*), whose Doppler width is one third of the laser's. Translational relaxation is not included in the model; this results in a small overprediction of the resonant background due to (R3) and of the positive component of the net interference.

The nascent distribution of HO produced by reaction (R3) is derived from *Cleveland*'s [1988] experimental measurements, obtained at a lower value of $P\Delta t$ (total pressure times delay between photolysis laser pulse and HO probe laser pulse) than were available to previous experimenters [*Rodgers et al.*, 1981; *Gericke and Comes*, 1980, 1982; *Gericke et al.*, 1981]. The *Cleveland* [1988] data fully characterize the vibrational and rotational distributions of each of the two fragments formed in reaction (R3); for our purposes, it is sufficient to sum the nascent populations of the two fragments in each of the two probed levels, relative to the total nascent population in all states. We calculated the fraction in $v''=0$ (0.645) from Cleveland's Table 4.4; the low-N fraction in $v''=0$ was taken as 80% of the upper limit given in Cleveland's Table 4.3; and the high-N fraction in $v''=0$ as the difference between the latter two. The low-N levels are not characterized by a well-defined temperature; therefore we obtained the fractional populations for our probed levels from Figures 4.5 and 4.6 of *Cleveland* [1988], which give $n_{N''}/(2J''+1)$ for HO associated with the "new" and "old" bonds in the reaction $O(^1D) + H_2{}^{18}O \rightarrow H^{18}O + H^{16}O$. The value of the nascent doppler width of HO from reaction (R4*a*) is that measured by *Gericke and Comes* [1981, 1982; *Gericke et al.*, 1981] for the Q_15 transition, and the effective relaxation rate coefficient of the hot rotational distribution due to H_2O is that of *Gericke and Comes* [1982].

For convenience, those rotationally cold levels which are not probed by the laser are lumped into a single state. Rotational hole-filling rate coefficients for each probed level are obtained by multiplying the rotational relaxation coefficient by the ratio of the total equilibrium population of levels other than the probed level to the equilibrium population of the probed level. For ambient HO without laser excitation the model gives no net transfer among these levels at thermal equilibrium; pulsed excitation is followed by relaxation to the same distribution. In contrast, the hot rotational levels in X $(v''=0)$ (populated by reaction (R3)) are treated as an additional single state, with one-way rotational relaxation paths to the probed and the nonprobed lower levels. Finally, in the A state, rotational relaxation from the initially excited levels is treated as one-way transfer to a lumped level, which is subject to all loss processes

except for rotational relaxation. Setting all of the rotational relaxation rate coefficients to zero gives a 9% decrease in the ambient HO signal, a 6% increase in the gross photochemical background, and a 16% increase in the net interference. These processes become more significant under time-delayed irradiation by two or more successive laser passes in the White cell from the same laser pulse.

In the absence of an accurate value for k_{Vi} in equation (5), we assume that the inclusion of both k_{Qli} and k_{Vi} leaves the first fraction in equation (5) nearly unchanged, although a very large value of k_{Vi} would invalidate this assumption.

Factors not considered in the single pass model include nonuniform laser-beam cross section (which would increase interference), as well as mode-chirping of the laser frequency across the HO absorption spectral profile during the laser pulse (which would decrease interference).

The kinetic model is run using the program Prex8 which we wrote in Tbasic (Trans Era Corporation) on an AT clone computer, in order to enable multiple runs under the conditions of Figures 6, 7, 11, and 12. Since this program lacks a predictor-corrector with step-size adjustment, it is run under progressively smaller step sizes until each of the model results, at the end of the laser pulse and at the end of the signal detection gate, are constant to within 1%. To check the accuracy of Prex8's structure, the model is also run under the same conditions using two formal kinetics programs, Pamol (X. Pan and R. J. O'Brien, unpublished data, 1990), which is similar to CHEMK [*Whitten and Hogo*, 1980], and Ssechem (W. H. Pan and R. J. O'Brien, unpublished). All three programs give results which agree.

The simulation of the multipass resonant background in FAGE2 uses the observed alternating laser beam diameters (0.6 and 0.4 cm), a typical delay of 15 ns between the overlapping beams, and an adjustable value for the common fractional spatial overlap between them (neglecting the fact that the common overlap is a larger fraction of the smaller beam, and vice versa). Since the diameters of the beams differ, it is necessary first to obtain values of the time-integrated fluorescence (photons cm^{-3}) emitted from each beam. The integrated fluorescence due to the second beam is found by subtraction of single-pass fluorescence from double-pass fluorescence. The time-integrated fluorescence from each beam is then multiplied by the respective emitting volume within the detector's field of view, and the results are summed to give the space-integrated fluorescence (photons). The latter steps are performed with 0.6 cm for the diameter of the first beam and 0.4 cm for the second, and vice versa, and the results are averaged. Up to this point, separate computations for ambient HO and for the resonant background have been maintained; here the step corresponding to physical measurement of their respective total values has been reached, and it is appropriate to normalize the resonant background to the ambient HO signal. For comparison with the experimental multipass/single-pass ratio the latter result is divided by the corresponding single-pass model result for 0.6-cm beam diameter. This process is repeated with adjustment of the spatial overlap until the model results agree with experiment.

Acknowledgments. A. R. Ravishankara was the first to point out the importance of HO A $(v'=0)$ quenching by isobutane in accounting for the positive slope of the experimental data in Figure 6. We are also indebted to G. P. Smith, D. R. Crosley, J. J. Valentini, M. I. Lester, and J. Barker for helpful discussions. We are grateful to G. P. Smith and D. R. Crosley who provided us with a copy of their paper prior to publication, to C. B. Cleveland for a copy of chapter 4 of her thesis, and to J. Greenberg at the National Center for Atmospheric Research who provided hydrocarbon analyses. This work was supported by National Science Foundation grant ATM-8615163, National Aeronautics and Space Administration grant NAG-1-697, and Environmental Protection Agency grant R81-3012. This is Environmental Sciences and Resources Program Publication 250.

REFERENCES

Altshuller, A. P., Ambient air hydroxyl radical concentrations: Measurements and model predictions, *J. Am. Pollut. Control Assoc., 39*, 704–708, 1989.

Bevington, P. R., *Data Reduction in Error Analysis for the Physical Sciences*, McGraw-Hill (New York), 1969.

Burris, J., J. J. Butler, T. J. McGee, and W. S. Heaps, Collisional deactivation rates for $A^2\Sigma^+(v'=1)$ state of OH, *Chem. Phys., 124*, 251–258, 1988.

Butler, J. E., L. D. Talley, G. K. Smith, and M. C. Lin, Rotational and vibrational energy distributions of $16OH(X^2\Pi)$ and $^{18}OH(X^2\Pi)$ produced in the reaction of $O(^1D)$ with H_2O and $H_2{}^{18}O$, *J. Chem. Phys., 74*, 4501–4508, 1981.

Carroll, M. A. et al., Aircraft measurements of NO_x over the eastern Pacific and continental United States and implications for ozone production, *J. Geophys. Res., 95*, 10,205–10,233, 1990.

Chan, C. Y., R. J. O'Brien, T. M. Hard, and T. B. Cook, Laser-excited fluorescence of the hydroxyl radical: Relaxation coefficients at atmospheric pressure, *J. Phys. Chem., 87*, 4966–4974, 1983.

Chan, C. Y., A. A. Mehrabzadeh, T. M. Hard, and R. J. O'Brien, Third-generation FAGE instrument for tropospheric hydroxyl radical measurement, *J. Geophys. Res., 95*, 18,569–18,576, 1990.

Cleveland, C. B., Spectroscopic and dynamic studies of oxygen and ozone chemistry, thesis, Cornell Univ., Ithaca, N. Y., 1988.

Comes, F. J., K. H. Gericke, and J. Manz, Energy partitioning in the reaction $^{16}O(^1D)+H_2{}^{18}O\rightarrow{}^{16}OH+{}^{18}OH$, IV, Microscopic probabilities for $^{16}OH+{}^{18}OH$ coincident pairs, *J. Chem. Phys., 75*, 2853–2863, 1981.

Copeland, R. A., M. J. Dyer, and D. R. Crosley, Rotational-level-dependent quenching of $A^2\Sigma^+$ OH and OD, *J. Chem. Phys., 82*, 4022–4032, 1985.

Copeland, R. A., M. L. Wise, and D. R. Crosley, Vibrational energy transfer and quenching of $OH(A^2\Sigma^+,v'=1)$, *J. Phys. Chem. 92*, 5710–5715, 1988.

Darnall, K., R. Atkinson, and J. N. Pitts, Jr., Rate constants for the reaction of the OH radical with selected alkanes at 300 K, *J. Phys. Chem. 82*, 1581–1584, 1978.

Davis, D. D., M. O. Rodgers, S. D. Fischer, and K. Asai, An experimental assessment of the O_3/H_2O interference problem in the detection of natural levels of OH via laser induced fluorescence, *Geophys. Res. Lett., 8*, 69–72, 1981*a*.

Davis, D. D., M. O. Rodgers, S. D. Fischer, and W. S. Heaps, A theoretical assessment of the O_3/H_2O interference problem in the detection of natural levels of OH via laser induced fluorescence, *Geophys. Res. Lett., 8*, 73–76, 1981*b*.

DeMore, W. B., M. J. Molina, S. P. Sander, D. M. Golden, R. F. Hampson, M. J. Kurylo, C. J. Howard, and A. R. Ravishankara, Chemical kinetics and photochemical data for use in stratospheric modeling, Rep. *JPL-NASA 87-41*, 98 pp., Jet Propulsion Lab., Pasadena, Calif., 1987.

Docker, M. P., A. Hodgson,, and J. P. Simons, Photodissociation of H_2O_2 at 248 nm: Translational anisotropy and OH product distributions, *Chem. Phys. Lett., 128*, 264–269, 1986.

Eisele, F. L., and D. J. Tanner, Ion-assisted tropospheric OH measurements, *J. Geophys. Res., 96*, 9295–9308, 1991.

Felton, C. C., J. C. Sheppard, and M. J. Campbell, Measurements

of the diurnal OH cycle by a ^{14}C-tracer method, *Nature, 335*, 53–55, 1988.

Gericke, K. H., and F. J. Comes, Energy partitioning in the reaction $O(^1D)+H_2O \rightarrow OH+OH$, *Chem. Phys. Lett., 74*, 63–66, 1980.

Gericke, K. H., and F. J. Comes, Energy partitioning in the reaction $O(^1D)+H_2O \rightarrow OH+OH$. The influence of $O(^1D)$ translational energy on the reaction rate constant, *Chem. Phys. Lett., 81*, 218–222, 1981.

Gericke, K. H., and F. J. Comes, Energy partitioning in the $O(^1D)+H_2O \rightarrow OH+OH$ reaction, V, Rotational relaxation of $OH(X^2\pi, v'', j'')$, *Chem. Phys., 65*, 113–121, 1982.

Gericke, K. H., F. J. Comes, and R. D. Levine, Energy partitioning in the reaction $^{16}O(^1D)+H_2{}^{18}O \rightarrow {}^{16}OH+{}^{18}OH$, II, The distribution of ^{16}OH and ^{18}OH, *J. Chem. Phys., 74*, 6106–6112, 1981.

Gericke, K. H., S. Klee, F. J. Comes, and R. N. Dixon, Dynamics of H_2O_2 photodissociation: OH product state and momentum distribution characterized by sub-Doppler and polarization spectroscopy, *J. Chem. Phys., 85*, 4463–4479, 1986.

German, K. R., Collision and quenching cross sections in the $A^2\Sigma^+$ state of OH and OD, *J. Chem. Phys., 64*, 4065–4068, 1976.

Hanabusa, M., C. C. Wang, S. Japar, D. K. Killinger, and W. Fisher, Pulsewidth dependence of ozone interference in the laser fluorescence measurement of OH in the atmosphere, *J. Chem. Phys., 66*, 2118–2120, 1977.

Hard, T. M., R. J. O'Brien, and T. B. Cook, Pressure dependence of fluorescent and photolytic interferences in HO detection by laser-excited fluorescence, *J. Appl. Phys., 51*, 3459–3464, 1980.

Hard, T. M., R. J. O'Brien, C. Y. Chan, and A. A. Mehrabzadeh, Tropospheric free radical determination by FAGE, *Environ. Sci. Technol., 18*, 768–777, 1984.

Hard, T. M., C. Y. Chan, A. A. Mehrabzadeh, W. H. Pan, and R. J. O'Brien, Diurnal cycle of tropospheric OH, *Nature, 322*, 617–620, 1986.

Hard, T. M., C. Y. Chan, A. A. Mehrabzadeh, and R. J. O'Brien, Pressure dependence of ozone interference in the laser fluorescence measurement of OH in the atmosphere: Comment, *Appl. Opt., 28*, 26–27, 1989.

Hewitt, C. N., and R. M. Harrison, Tropospheric concentrations of the hydroxyl radical–A review, *Atmos. Environ., 19*, 545–554, 1985.

Keyser, L. F., Absolute rate constant of the reaction $OH + H_2O_2 \rightarrow H_2O + O_2$, *J. Phys. Chem., 85*, 3667–3673, 1981.

Logan, J. A., M. J. Prather, S. C. Wofsy, and M. B. McElroy, Tropospheric chemistry: A global perspective, *J. Geophys. Res., 86*, 7210–7254, 1981.

Luntz, A. C., Chemical dynamics of the reactions of $O(^1D_2)$ with saturated hydrocarbons, *J. Chem. Phys., 73*, 1143–1152, 1980.

McGee, T. J., and T. J. McIlrath, Absolute OH absorption cross sections (for lidar measurements), *J. Quant. Spectrosc. Radiat. Transfer, 32*, 179–184, 1984.

Michaud, P., G. Paraskevopoulos, and R. J. Cvetanović, Relative rates of the reactions of $O(^1D2)$ atoms with alkanes and cycloalkanes, *J. Phys. Chem., 78*, 1457–1461, 1974.

Migliore, H. J., and B. S. Bishop, Computational flow analysis for trace element measurement, in *Computers in Engineering 1988, 3*, pp. 507–512, American Society of Mechanical Engineers, N.Y., 1988.

Molina, L. T., and M. J. Molina, Absolute absorption cross sections of ozone in the 185- to 350-nm wavelength range, *J. Geophys. Res., 91*, 14,501–14,508, 1986.

Ortgies, G., K. H. Gericke, and F. J. Comes, Optical measurements of tropospheric hydroxyl with lasers, *Z. Naturforsch., 36a*, 177–183, 1981.

Paraskevopoulos, G., and R. J. Cvetanović, Reaction of the excited oxygen atoms ($O(^1D_2)$) with isobutane, *J. Chem. Phys., 50*, 590–599, 1969.

Pickett, H. M., G. M. Bradley, and H. L. Strauss, A new White type multiple pass absorption cell, *Appl. Opt. 9*, 2397–2398, 1970.

Platt, U., M. Rateike, W. Junkermann, J. Rudolph, and D. H. Ehhalt, New tropospheric OH measurements, *J. Geophys. Res., 93*, 5159–5166, 1988.

Rodgers, M. O., K. Asai, and D. D. Davis, OH rotational quantum state distributions and relaxation efficiencies for the reaction system $O(^1D)+H_2O \rightarrow 2OH$, *Chem. Phys. Lett., 78*, 246–252, 1981.

Rodgers, M. O., J. D. Bradshaw, S. T. Sandholm, S. KeSheng, and D. D. Davis, A two-lambda laser-induced fluorescence field instrument for ground-based and airborne measurements of atmospheric OH, *J. Geophys. Res., 90*, 12,819–12,834, 1985.

Shirinzadeh, B., C. C. Wang, and D. Q. Deng, Pressure dependence of ozone interference in the laser fluorescence measurement of OH in the atmosphere, *Appl. Opt., 26*, 2102–2105, 1987*a*.

Shirinzadeh, B., C. C. Wang, and D. Q. Deng, Diurnal variation of the OH concentration in ambient air, *Geophys. Res. Lett., 14*, 123–126, 1987*b*.

Smith, G. P., and D. R. Crosley, A photochemical model of interference effects in laser detection of tropospheric OH, *J. Geophys. Res., 95*, 16,427–16,442, 1990.

Stephens, R. D., Quenching of $OH(A^2\Sigma^+)$ by alkanes and chlorofluorocarbons at room temperature, *J. Phys. Chem., 1985*, 2630–3635, 1985.

Vaghjiani, G. L., and A. R. Ravishankara, Quenching of OD ($A^2\Sigma^+$, $v'=0$ and 1) by various gases, *J. Chem. Phys., 87*, 7050–7058, 1987.

Wang, C. C., and L. I. Davis, Comments on "Theoretical and experimental assessment of the O_3/H_2O interference problem in the detection of OH" by Davis et al., *Geophys. Res. Lett., 9*, 98–100, 1982.

Wang, C. C., L. I. Davis, P. M. Seltzer, and R. Munoz, Improved airborne measurements of OH in the atmosphere using the technique of laser-induced fluorescence, *J. Geophys. Res., 86*, 1181–1186, 1981.

Whitten, G. Z., and H. Hogo, Modeling of simulated smog with kinetic mechanisms–CHEMK, U. S. Environ. Prot. Agency, *Rep. EPA-600/3-80-028b*, Washington, D. C., 1980.

Wysong, I. J., J. B. Jeffries, and D. R. Crosley, Quenching of $A^2\Sigma^+$ OH at 300 K by several colliders, *J. Chem. Phys., 92*, 5218–5222, 1990.

C. Y. Chan, T. M. Hard, A. A. Mehrabzadeh, and R. J. O'Brien, Chemistry Department and Environmental Sciences and Resources Doctoral Program, Portland State University, Portland, Oregon 97207.

(Received February 12, 1990;
revised June 17,1991;
accepted June 20, 1991.)